

# Analyses of pion-nucleon elastic scattering amplitudes up to $O(p^4)$ in extended-on-mass-shell subtraction scheme

Yun-Hua Chen<sup>a,b</sup>, De-Liang Yao<sup>a</sup>, H. Q. Zheng<sup>a</sup>

<sup>a</sup> Department of Physics and State Key Laboratory of Nuclear Physics and Technology, Peking University, Beijing 100871, China P.R.

<sup>b</sup> Institute of High Energy Physics, CAS, P.O. Box 918(4), Beijing 100049, China<sup>1</sup>

## Abstract

We extend the analysis of elastic pion-nucleon scattering up to  $O(p^4)$  level using the extended-on-mass-shell subtraction scheme within the framework of covariant baryon chiral perturbation theory. Numerical fits to partial wave phase shift data up to  $\sqrt{s} = 1.13$  GeV are performed to pin down the free low energy constants. A good description of the existing phase shift data is achieved. We find a good convergence for the chiral series at  $O(p^4)$ , considerably improved with respect to the  $O(p^3)$ -level analyses found in previous literature. Also, the leading order contribution from explicit  $\Delta(1232)$  resonance and partially-included  $\Delta(1232)$  loop contribution are included to describe the phase shift data up to  $\sqrt{s} = 1.20$  GeV. As phenomenological applications, we investigate chiral corrections to the Goldberger-Treiman relation and find that it converges rapidly, and the  $O(p^3)$  correction is found to be very small:  $\simeq 0.2\%$ . We also get a reasonable prediction of the pion-nucleon sigma term  $\sigma_{\pi N}$  up to  $O(p^4)$  by performing fits including both the pion-nucleon partial wave phase shift data and the lattice QCD data. We report that  $\sigma_{\pi N} = 52 \pm 7$  MeV from the fit without  $\Delta(1232)$ , and  $\sigma_{\pi N} = 45 \pm 6$  MeV from the fit with explicit  $\Delta(1232)$ .

**Keywords:** pion-nucleon scattering, chiral perturbation theory, partial wave analysis, Goldberger-Treiman relation, pion-nucleon sigma term

## 1. Introduction

Pion-nucleon scattering is an important process for the understanding of chiral QCD dynamics and the interpretation of some prominent phenomenology of strong interactions [1]. Many efforts have been made to study it. However, unlike the successfulness of chiral perturbation theory ( $\chi$ PT) [2, 3] in the pure meson sector, a chiral expansion in the pion-nucleon scattering amplitude suffers from the power counting breaking (PCB) problem in the traditional subtraction  $\overline{MS} - 1$  scheme [4]. Many proposals have been made to remedy this problem, e.g., heavy baryon (HB) chiral perturbation theory [5], infrared regularization (IR) scheme [6], extended on mass shell (EOMS) scheme [7, 8], etc..

As a successful nonrelativistic effective field theory, HB chiral perturbation theory rebuilds a power counting rule through simultaneous expansions in terms of  $1/m_N$  and external momentums. The pion-nucleon scattering has been investigated up to  $O(p^3)$  [9, 10] and  $O(p^4)$  [11] with HB approach. Though the description of  $\pi$ -N scattering phase shift data is well described near the threshold region, the nonrelativistic expansion encounters the problem of convergence in many cases [6, 11–13], e.g. the scalar form factor of the nucleon does not converge in the region close to the two-pion threshold  $t = 4M_\pi^2$  [6, 13].

On the other side, in the framework of relativistic chiral theory, one may conclude that all the power-violating terms are polynomials and can thus be absorbed in the low energy constants from the effective Lagrangian [14, 15]. Hence the IR prescription and EOMS scheme are proposed to retain both correct power counting and covariance. Nevertheless, they are different in practice when removing chiral polynomials, the former subtracts all the so-called

<sup>1</sup>Current address.

Email addresses: chenyh@ihep.ac.cn (Yun-Hua Chen), yaodeliang@pku.edu.cn (De-Liang Yao), zhenghq@pku.edu.cn (H. Q. Zheng)

infrared regular part of the loop integrals, which is always an infinite chiral polynomial of different order, while the latter only cancels the finite PCB terms. In Refs. [16–18] the pion-nucleon scattering amplitude is analyzed within IR prescription. In Ref. [16], the  $O(p^4)$  calculation was carried out and the analytic property of the amplitude was discussed. In Refs. [17, 18] the  $O(p^3)$  calculation result was used to fit the phase shift data. However, it has been shown that the pion-nucleon amplitude in IR prescription is scale-dependent [16] and suffers from an unphysical cut at  $u=0$  [18]. Additionally, a huge violation of Goldberger-Treiman (GT) relation shows up [18], which queries the applicability of covariant baryon chiral perturbation theory. Hence these problems lead to the application of the EOMS scheme.

The EOMS scheme provides a good solution to the PCB problem in the sense that it faithfully respects the analytic structure of the original amplitudes, e.g., see Ref. [19], and being scale independent for merely making an additional subtraction of a polynomial of PCB terms with respect to the traditional subtraction. A first attempt of the EOMS scheme on pion-nucleon scattering was made up to  $O(p^3)$  level by Alarcón et al. [20]. Remarkably, achievements in the description of violation of the GT relation [21] and the pion-nucleon sigma term [22] are obtained. However, as pointed in Ref. [23], the size of the  $O(p^3)$  contribution can be very large and comparable to those given by the lower-order terms even at very low energies above threshold. Thus, the applicability of EOMS scheme to describe the partial wave phase shift at  $O(p^3)$  seems to be questionable. The authors of Refs. [20, 23] solve the problem by explicitly including the contribution of  $\Delta(1232)$  resonance.

In this paper we extend the analysis up to  $O(p^4)$ , and settle down the convergence problem occurred in the  $O(p^3)$ -level analysis, even when the  $\Delta(1232)$  resonance is absent. Compared with the  $O(p^4)$ -IR results in Ref. [16], the pion-nucleon scattering amplitude presented here is the first analytic and complete  $O(p^4)$  result. Especially, we pay great attention to the subtraction of PCB terms, such that the “threshold divergence” problem first pointed out by [24] within the IR prescription never occurs. We perform fits to partial wave phase shift data and determine all the LECs involved. Besides, the leading order contribution from an explicit  $\Delta(1232)$  resonance and partially-included  $\Delta(1232)$  loop contribution are included to describe phase shift data up to energies just below the resonance region.

A phenomenological discussion is also made based on the pion-nucleon scattering amplitude we obtain. We have mainly studied the Goldberger-Treiman (GT) relation and the pion-nucleon sigma term  $\sigma_{\pi N}$ . The GT relation violation is a basic quantity to test the applicability of EOMS-B $\chi$ PT to the pion-nucleon system. Hence we calculate it up to  $O(p^3)$ . The prediction of the violation is in good agreement with other determinations [25, 26], and its chiral series converges rapidly. The analysis on  $\sigma_{\pi N}$  is important to understand the origin of the mass of the ordinary matter and can be useful for the study of the supersymmetric dark matter [27, 28]. Taking both pion-nucleon phase shift and the lattice QCD data into consideration, we give a reasonable prediction for the pion-nucleon sigma term:  $\sigma_{\pi N} = 52 \pm 7$  MeV from the fit without  $\Delta(1232)$ , and  $\sigma_{\pi N} = 45 \pm 6$  MeV from the fit with an explicit  $\Delta(1232)$ . The first one is smaller than the  $O(p^3)$  result given by Ref. [20] but larger than the recent  $O(p^4)$  result in Ref. [29], while the latter is in reasonable agreement with previous results found in the literature [29–31].

## 2. Theoretical discussions on $\pi N \rightarrow \pi N$ in EOMS scheme

### 2.1. Kinematics and effective Lagrangian

In the isospin limit, the standard decomposition of the elastic  $\pi$ - $N$  amplitude reads [4, 16],

$$T_{\pi N}^{a'a} = \chi_{N'}^\dagger \left\{ \delta_{a'a} T^+ + \frac{1}{2} [\tau_{a'}, \tau_a] T^- \right\} \chi_N, \quad T^\pm = \bar{u}(p', s') \left[ A^\pm + \frac{1}{2} (\not{q}' + \not{q}) B^\pm \right] u(p, s), \quad (1)$$

where  $p, q(p', q')$  denote the momenta of the incoming (outgoing) nucleons and pions, respectively, and  $a(a')$  stands for the isospin index of the incoming (outgoing) pion, see Fig.1.  $\tau_{a'}, \tau_a$  are Pauli matrices and  $\chi_{N'}, \chi_N$  are the isospinors of the nucleons. For on-shell elastic scatterings,  $p^2 = p'^2 = m_N^2, q^2 = q'^2 = M_\pi^2$  and the Mandelstam variables  $s, t$  and  $u$  fulfill  $s + t + u = 2m_N^2 + 2M_\pi^2$ . Eq. (1) can be written in an alternative form through the replacement of  $A$  by  $D = A + \nu B$  with  $\nu = \frac{s-u}{4m_N}$ :

$$T^\pm = \bar{u}(p', s') \left[ D^\pm + \frac{i}{2m_N} \sigma^{\mu\nu} q'_\mu q_\nu B^\pm \right] u(p, s). \quad (2)$$

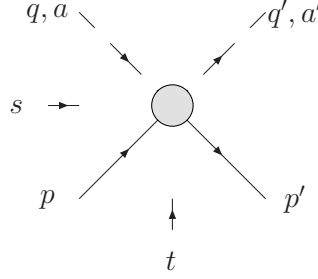


Figure 1: Kinematics of elastic  $\pi$ -N scattering.  $p, q$  ( $p', q'$ ) denote the momenta of the incoming (outgoing) nucleons and pions, respectively, and  $a$  ( $a'$ ) stands for the isospin index of the incoming (outgoing) pion.

Since the leading order contribution of A and B may cancel each other, one should better use D and B to perform the low energy expansion of the scattering amplitude when extracting the PCB terms. Our calculation of the  $\pi$ -N scattering amplitude up to  $O(p^4)$  level demands the corresponding calculation of  $D^\pm$  and  $B^\pm$  up to  $O(p^4)$  and  $O(p^2)$ , respectively.

In chiral perturbation theory, each graph is assigned an overall chiral order  $D$ , which means the graph is of size  $(p/\Lambda)^D$ , where one has the soft scale  $p \ll \Lambda$  and  $\Lambda$  stands for a “high energy scale”, i.e., the breakdown scale of the theory. For processes containing one baryon in the initial and final states, the chiral order for a given graph with  $L$  loops,  $V_n$   $n$ -th order vertices,  $N_M$  meson propagators and  $N_B$  baryon propagators, is given by

$$D = 4L + \sum_n nV_n - 2N_M - N_B. \quad (3)$$

The effective Lagrangian relevant to the one-nucleon sector consists of  $\pi$ -N and purely mesonic Lagrangian,

$$\mathcal{L}_{eff} = \mathcal{L}_{\pi N}^{(1)} + \mathcal{L}_{\pi N}^{(2)} + \mathcal{L}_{\pi N}^{(3)} + \mathcal{L}_{\pi N}^{(4)} + \dots + \mathcal{L}_{\pi\pi}^{(2)} + \mathcal{L}_{\pi\pi}^{(4)} + \dots, \quad (4)$$

where the superscripts denote the chiral order. The lowest  $\pi$ -N Lagrangian takes the standard form

$$\mathcal{L}_{\pi N}^{(1)} = \bar{N} \left\{ i \not{D} - m + \frac{1}{2} g \not{\gamma} \gamma^5 \right\} N. \quad (5)$$

The nucleons are described by an isospin doublet as  $N = (n, p)^T$ , and the covariant derivative  $D_\mu$  acting on it is defined as  $D_\mu = \partial_\mu + \Gamma_\mu$ , with

$$\Gamma_\mu = \frac{1}{2} \left[ u^\dagger (\partial_\mu - i r_\mu) u + u (\partial_\mu - i l_\mu) u^\dagger \right], \quad (6)$$

where  $l_\mu$  and  $r_\mu$  are constructed from the external vector and axial vector currents as  $l_\mu = v_\mu - a_\mu$  and  $r_\mu = v_\mu + a_\mu$ . The Goldstone bosons are collected in a  $2 \times 2$  matrix-valued field  $u$  in the so-called exponential parametrization

$$u_\mu = i \left[ u^\dagger (\partial_\mu - i r_\mu) u - u (\partial_\mu - i l_\mu) u^\dagger \right], \quad u = \exp \left( \frac{i \vec{\tau} \cdot \vec{\pi}}{2F} \right), \quad (7)$$

with  $\vec{\tau}$  being the Pauli matrices. The parameters appearing in this lowest-order  $\pi$ -N Lagrangian,  $m$ ,  $F$ , and  $g$  are the bare values of the nucleon mass, the pion decay constant and the axial charge, respectively.

For the complete form of  $\mathcal{L}_{\pi N}^{(2)}$ ,  $\mathcal{L}_{\pi N}^{(3)}$  and  $\mathcal{L}_{\pi N}^{(4)}$ , we refer to Ref. [32]. Here we only write down the terms which are

relevant to our calculation:

$$\mathcal{L}_{\pi N}^{(2)} = c_1 \langle \chi_+ \rangle \bar{N} N - \frac{c_2}{4m^2} \langle u^\mu u^\nu \rangle (\bar{N} D_\mu D_\nu N + h.c.) + \frac{c_3}{2} \langle u^\mu u_\mu \rangle \bar{N} N - \frac{c_4}{4} \bar{N} \gamma^\mu \gamma^\nu [u_\mu, u_\nu] N, \quad (8)$$

$$\begin{aligned} \mathcal{L}_{\pi N}^{(3)} = & \bar{N} \left\{ -\frac{d_1 + d_2}{4m} ([u_\mu, [D_\nu, u^\mu] + [D^\mu, u_\nu]] D^\nu + h.c.) \right. \\ & + \frac{d_3}{12m^3} ([u_\mu, [D_\nu, u_\lambda]] (D^\mu D^\nu D^\lambda + \text{sym.}) + h.c.) + i \frac{d_5}{2m} ([\chi_-, u_\mu] D^\mu + h.c.) \\ & + i \frac{d_{14} - d_{15}}{8m} (\sigma^{\mu\nu} \langle [D_\lambda, u_\mu] u_\nu - u_\mu [D_\nu, u_\lambda] \rangle D^\lambda + h.c.) \\ & \left. + \frac{d_{16}}{2} \gamma^\mu \gamma^5 \langle \chi_+ \rangle u_\mu + \frac{id_{18}}{2} \gamma^\mu \gamma^5 [D_\mu, \chi_-] \right\} N, \end{aligned} \quad (9)$$

$$\begin{aligned} \mathcal{L}_{\pi N}^{(4)} = & \bar{N} \left\{ e_{14} \langle h_{\mu\nu} h^{\mu\nu} \rangle - \frac{e_{15}}{4m^2} (\langle h_{\lambda\mu} h^\lambda{}_\nu \rangle D^{\mu\nu} + h.c.) + \frac{e_{16}}{48m^4} (\langle h_{\lambda\mu} h_{\nu\rho} \rangle D^{\lambda\mu\nu\rho} + h.c.) \right. \\ & + \frac{ie_{17}}{2} [h_{\lambda\mu}, h^\lambda{}_\nu] \sigma^{\mu\nu} - \frac{ie_{18}}{8m^2} ([h_{\lambda\mu}, h_{\nu\rho}] \sigma^{\mu\nu} D^{\lambda\rho} + h.c.) + e_{19} \langle \chi_+ \rangle \langle u \cdot u \rangle \\ & - \frac{e_{20}}{4m^2} (\langle \chi_+ \rangle \langle u_\mu u_\nu \rangle D^{\mu\nu} + h.c.) + \frac{ie_{21}}{2} \langle \chi_+ \rangle [u_\mu, u_\nu] \sigma^{\mu\nu} + e_{22} [D_\mu, [D^\mu, \langle \chi_+ \rangle]] \\ & - \frac{ie_{35}}{4m^2} (\langle \tilde{\chi}_- h_{\mu\nu} \rangle D^{\mu\nu} + h.c.) + ie_{36} \langle u_\mu [D^\mu, \tilde{\chi}_-] \rangle - \frac{e_{37}}{2} [u_\mu, [D_\nu, \tilde{\chi}_-]] \sigma^{\mu\nu} + e_{38} \langle \chi_+ \rangle \langle \chi_+ \rangle \\ & \left. + \frac{e_{115}}{4} \langle \chi_+^2 - \chi_-^2 \rangle - \frac{e_{116}}{4} (\langle \chi_-^2 \rangle - \langle \chi_- \rangle^2 + \langle \chi_+^2 \rangle - \langle \chi_+ \rangle^2) \right\} N, \end{aligned} \quad (10)$$

where the  $c_i$ ,  $d_j$  and  $e_k$  are the low energy constants. The new symbols appearing here are defined as follows,

$$\begin{aligned} \chi^\pm &= u^\dagger \chi u^\dagger \pm u \chi^\dagger u, \\ h_{\mu\nu} &= [D_\mu, u_\nu] + [D_\nu, u_\mu], \\ \tilde{\chi}_\pm &= \chi_\pm - \frac{1}{2} \langle \chi_\pm \rangle, \\ D_{\alpha\beta\dots\omega} &= \{D_\alpha D_\beta \dots D_\omega + \text{sym.}\}. \end{aligned} \quad (11)$$

Here  $\chi = \mathcal{M} = \text{diag}(M^2, M^2)$  and  $M$  is the bare pion mass. In the pure meson sector, the relevant terms of  $\mathcal{L}_{\pi\pi}^{(2)}$  and  $\mathcal{L}_{\pi\pi}^{(4)}$  are given by

$$\begin{aligned} \mathcal{L}_{\pi\pi}^{(2)} &= \frac{F^2}{4} \langle u^\mu u_\mu + \chi_+ \rangle, \\ \mathcal{L}_{\pi\pi}^{(4)} &= \frac{1}{8} l_4 \langle u^\mu u_\mu \rangle \langle \chi_+ \rangle + \frac{1}{16} (l_3 + l_4) \langle \chi_+ \rangle^2, \end{aligned} \quad (12)$$

and  $l_3, l_4$  are low energy constants that will appear in our calculation, too. It is noticed that throughout this paper  $m, M, g, F$  represent the bare quantities for nucleon mass, pion mass, axial coupling constant and pion decay constant, respectively whereas  $m_N, M_\pi, g_A, F_\pi$  the corresponding physical quantities. For the kinematic region close to the  $\pi N$  threshold, one has

$$\frac{\sigma}{\Lambda^2} \ll 1, \frac{t}{\Lambda^2} \ll 1, \frac{M_\pi}{\Lambda} \ll 1,$$

or equivalently

$$\frac{\nu}{\Lambda} \ll 1, \frac{\nu_B}{\Lambda} \ll 1, \frac{M_\pi}{\Lambda} \ll 1,$$

where  $\sigma = s - m_N^2$ ,  $\nu = \frac{s-u}{4m_N}$ ,  $\nu_B = \frac{t-2M_\pi^2}{4m_N}$ . Here the high energy scale  $\Lambda = \{4\pi F_\pi, m_N, m_\Delta, m_\Delta - m_N\}$  with  $m_\Delta$  the mass of  $\Delta(1232)$ . Hence  $\sigma, t, M_\pi$  (or  $\nu, \nu_B, M_\pi$ ) are adopted as expansion parameters, and

$$\sigma \sim O(p), t \sim O(p^2), M_\pi \sim O(p), \nu \sim O(p), \nu_B \sim O(p^2), m_N \sim O(p^0), m_\Delta \sim O(p^0), m_\Delta - m_N \sim O(p^0). \quad (13)$$

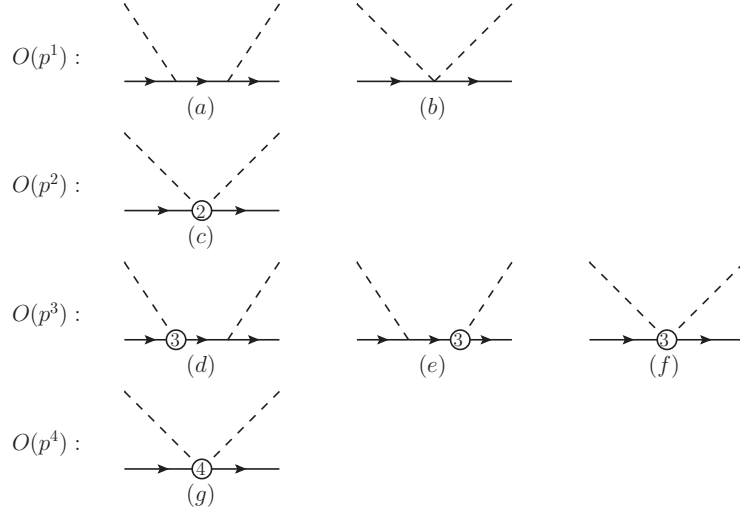


Figure 2: Tree graphs for  $\pi$ -N scattering up to  $O(p^4)$ . The solid lines correspond to nucleons, while the dashed lines represent pions. The vertices with circled 2, 3 and 4 stem from  $\mathcal{L}_{\pi N}^{(2)}$ ,  $\mathcal{L}_{\pi N}^{(3)}$  and  $\mathcal{L}_{\pi N}^{(4)}$ , respectively. The nucleon propagates with  $m_4 = m - 4c_1 M^2 - 2(8e_{38} + e_{115} + e_{116})$ . Crossed diagrams for (a), (d) and (e) are not shown.

## 2.2. Tree amplitudes

We show all the tree graphs which contribute up to  $O(p^4)$  in Fig. 2 according to the power counting rule given by Eq. (5), and list their contributions to  $D^\pm$  and  $B^\pm$  in Appendix B separately. The nucleon propagates with a mass parameter  $m_4 = m - 4c_1 M^2 - 2(8e_{38} + e_{115} + e_{116})M^4$  instead of  $m$ , so that the graphs with mass insertions, generated by  $c_1 \langle \chi_+ \rangle$  in  $\mathcal{L}_{\pi N}^{(2)}$  and  $e_{38} \langle \chi_+ \rangle \langle \chi_+ \rangle + \frac{e_{115}}{4} \langle \chi_+^2 - \chi_-^2 \rangle - \frac{e_{116}}{4} (\langle \chi_-^2 \rangle - \langle \chi_- \rangle^2 + \langle \chi_+^2 \rangle - \langle \chi_+ \rangle^2)$  in  $\mathcal{L}_{\pi N}^{(4)}$ , in the nucleon propagators are automatically considered. For convenience, one can classify the tree graphs into two categories: Born-terms and contact terms. In Fig. 2 contributions from Born-term graphs, (a), (d) and (e), and their crossed diagrams can be summed and rewritten concisely in terms of the  $A$  and  $B$  functions as

$$\begin{aligned} A^\pm &= A(s) \pm A(u), & A(s) &= \frac{g_2^2}{4F^2} \frac{s - m_N^2}{s - m_4^2} (m_4 + m_N), \\ B^\pm &= B(s) \mp B(u), & B(s) &= -\frac{g_2^2}{4F^2} \frac{s + 2m_N m_4 + m_N^2}{s - m_4^2}, \end{aligned} \quad (14)$$

with<sup>2</sup>  $m_4 = m - 4c_1 M^2 - 2(8e_{38} + e_{115} + e_{116})M^4$  and  $g_2 = g + 2M^2(2d_{16} - d_{18})$ . Meanwhile, the rest are contact term graphs without crossed diagrams, and the sum of them is

$$\begin{aligned} D^+ &= -\frac{4\hat{c}_1 M^2}{F^2} + \frac{\hat{c}_2 (16m_N^2 v^2 - t^2)}{8F^2 m^2} + \frac{\hat{c}_3 (2M_\pi^2 - t)}{F^2} + \frac{4}{F_\pi^2} \left\{ e_{14} (2M_\pi^2 - t)^2 + 2e_{15} (2M_\pi^2 - t) v^2 + 4e_{16} v^4 \right\}, \\ D^- &= \frac{v}{2F^2} + \frac{2v}{F_\pi^2} \left\{ 2(d_1 + d_2 + 2d_5)M_\pi^2 - (d_1 + d_2)t + 2d_3 v^2 \right\}, \\ B^+ &= \frac{4(d_{14} - d_{15})vm_N}{F_\pi^2}, \quad B^- = \frac{1}{2F^2} + \frac{2\hat{c}_4 m_N}{F^2} + \frac{8m_N}{F_\pi^2} \left\{ e_{17} (2M_\pi^2 - t) + 2e_{18} v^2 \right\}. \end{aligned} \quad (15)$$

Note that in the graphs of  $O(p^3)$  and  $O(p^4)$  shown in Fig. 2, the bare constants can be replaced by the physical ones, since the distinction is beyond the accuracy of our calculation. Such replacements have been done in Eqs. 15 and

<sup>2</sup>As for the  $O(p^4)$  effective Lagrangian, we adopt the conventions of Ref. [32], so  $m_4$  differs from the one in [16], where  $e_1^{BL} = -2(8e_{38} + e_{115} + e_{116})$ .

Appendix B, where the  $O(p^3)$  and  $O(p^4)$  contributions are expressed only by physical parameters. According to the discussion in Ref. [11], the terms proportional to  $e_k$  ( $k = 19, 20, 21, 22, 35, 36, 37, 38$ ) only amount to quark mass corrections of  $c_i$  ( $i = 1, 2, 3, 4$ ), hence here we have already adopted in Eq. (15) the following combinations of LECs,

$$\begin{aligned}\hat{c}_1 &= c_1 - 2M^2(e_{22} - 4e_{38}) , & \hat{c}_2 &= c_2 + 8M^2(e_{20} + e_{35}) , \\ \hat{c}_3 &= c_3 + 4M^2(2e_{19} - e_{22} - e_{36}) , & \hat{c}_4 &= c_4 + 4M^2(2e_{21} - e_{37}) .\end{aligned}\quad (16)$$

### 2.3. Loop amplitudes

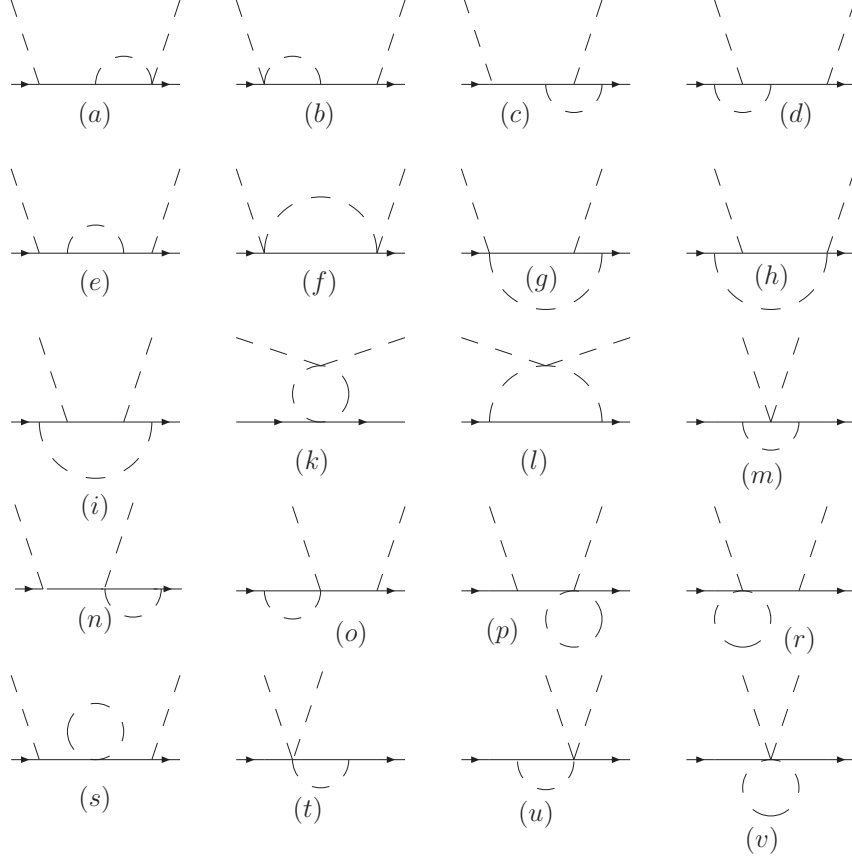


Figure 3: Loop graphs contributing to  $\pi$ -N scattering at  $O(p^3)$ . The nucleon propagates with  $m_4 = m - 4c_1 M^2 - 2(8e_{38} + e_{115} + e_{116})$ . Crossed graphs for (a)–(i) and (n)–(s) are not shown.

To carry out the calculation on  $\pi N \rightarrow \pi N$  process up to  $O(p^4)$  level, one ought to include  $O(p^3)$  and  $O(p^4)$  loop corrections with the corresponding Feynman diagrams shown in Fig. 3 and Fig 4, respectively. The  $O(p^4)$  loop graphs in Fig 4 are simply obtained from the graphs in Fig. 3 involving even number of pions by replacing one of the  $O(p)$  vertices with corresponding  $O(p^2)$  vertices. The results – in which no subtractions have yet been performed – are displayed in Appendix C.2 and Appendix C.3. There the  $O(p^3)$  loop results are listed explicitly for the sake of completeness. The definition of the loop functions is very similar to that in Ref. [16], which is presented in Appendix C.1. We have checked that our  $O(p^3)$  loop results agree with those in Ref. [23] except a few terms due to the reason that we have chosen exponential parametrization instead of sigma parametrization for the pion fields<sup>34</sup>.

<sup>3</sup>All the terms proportional to  $I_B^{(2)}$  in Ref. [16] should be reversed in sign, as it is first pointed out by Ref. [18].

<sup>4</sup>The physical pion-nucleon scattering amplitudes up to  $O(p^3)$  here and in Ref. [23] are the same and are independent of parametrization.

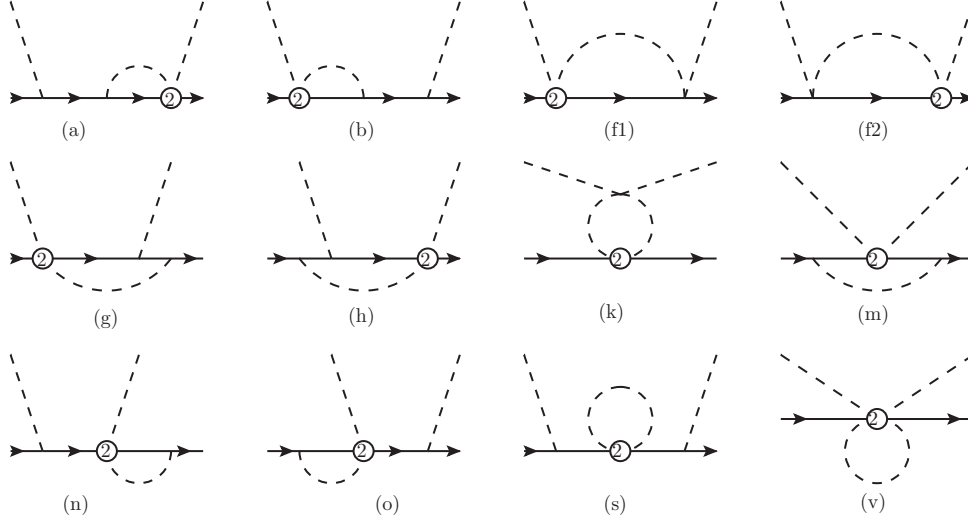


Figure 4: Loop graphs contributing to  $\pi$ -N scattering at  $O(p^4)$ . The vertex with circled '2' stems from  $\mathcal{L}_{\pi N}^{(2)}$ . The nucleon propagates with  $m_4 = m - 4c_1 M^2 - 2(8e_{38} + e_{115} + e_{116})$ . Crossed graphs are not shown.

To our knowledge, the  $O(p^4)$  loop contributions shown here are the first analytic and complete calculation results, and one can consult in Ref. [11] for the  $O(p^4)$  results within heavy baryon  $\chi$ PT and in Ref. [16] for the  $O(p^4)$  results within infrared regularization. In Ref. [16] special technical simplification of calculation is adopted, here we refer the readers to section 6 there for details.

It must be emphasized that the parameter  $m$  in both  $O(p^3)$  and  $O(p^4)$  loop results should be understood as  $m_4 = m - 4c_1 M^2 - 2(8e_{38} + e_{115} + e_{116})M^4$  for the following reasons [33]:

- All loop diagrams with contact interaction insertions in the nucleon propagators are summed up automatically;
- When performing renormalization, one can directly set  $m_4 = m_N$  in the one-loop results up to  $O(p^4)$  level, since corrections are at least of two-loop order (the lowest chiral order of two-loop contributions is naively  $O(p^5)$ ).

#### 2.4. EOMS scheme and PCB terms

Since the nucleon mass  $m_N$  is nonzero in the chiral limit, the necessary power counting rule for an effective theory breaks down, namely PCB problem occurs. To remedy the PCB problem we adopt the EOMS scheme proposed by T. Fuchs et al. [8], which suggests performing renormalization in two steps: the first traditional  $\overline{\text{MS}}$ -1 subtraction to cancel the ultraviolet divergencies and then EOMS subtraction to remove the PCB terms. The EOMS subtraction is remarkable in the sense that the renormalized  $\pi N \rightarrow \pi N$  amplitude will possess good analytic and correct power counting properties since the PCB terms are polynomials of quark masses and momenta and are absorbed in the LECs eventually. Especially, as proved by Becher and Leutwyler [6], the PCB terms stem from the regular part of the loop integrals, which allows us a simple way to obtain the PCB terms if we have known all the regular parts of the loop integrals needed – these are shown in Appendix D.

Taking the  $O(p^3)$  loop amplitude for example, one first changes the amplitude in  $A, B$  form to  $D, B$  functions<sup>5</sup> and reduces them to expressions only containing scalar one-loop integrals. Then those scalar one-loop integrals are substituted by their regular parts to a given order, and a chiral expansion in terms of small quantities like  $M, t, \sigma = s - m^2$  is performed<sup>6</sup>. Finally, for the total  $O(p^3)$  loop amplitude, the series whose chiral order are lower than  $O(p^3)$  are regarded as PCB terms which read

<sup>5</sup>In Ref. [16] the fact that the leading contribution from  $A$  and  $B$  cancels, while not for  $D$  and  $B$ , is pointed out.

<sup>6</sup>One can also chose  $\sigma = s - s_{th}$ , with  $s_{th} = (m + M)^2$ , as expanding parameter like Ref. [24], here we follow Ref. [4].

$$\begin{aligned}
D_{PCB}^{(3)+} &= \frac{1}{64F^4m\pi^2\sigma^2} \left\{ 6g^2m^2M^2\sigma^2 + 2\sigma^4 + g^4 \left[ 2m^4(10M^4 - 7M^2t + t^2) + 3m^2(-7M^2 + 3t)\sigma^2 + \sigma^4 \right] \right\}, \\
D_{PCB}^{(3)-} &= \frac{g^4m}{64F^4\pi^2\sigma^2} \left\{ \sigma^2(-2M^2 + t + 2\sigma) - 2m^2(2M^2 - t)(2M^2 - t + 2\sigma) \right\}, \\
B_{PCB}^{(3)+} &= \frac{g^4m^4}{8F^4\pi^2\sigma^2} (2M^2 - t + 2\sigma), \quad B_{PCB}^{(3)-} = \frac{g^2m^2}{32F^4\pi^2\sigma^2} \left\{ 5\sigma^2 + g^2 \left[ 4m^2(-5M^2 + t) + 3\sigma^2 \right] \right\}. \quad (17)
\end{aligned}$$

The same procedure can be taken to extract the PCB terms of the total  $O(p^4)$  loop amplitude,

$$\begin{aligned}
D_{PCB}^{(4)+} &= \frac{1}{1152F^4\pi^2\sigma^3} \left\{ 864c_1g^2m^2M^2\sigma^3 + \left[ 16c_4 - (9c_2 - 216c_3 + 272c_4)g^2 \right] m^2(t - 2M^2)\sigma^3 \right. \\
&\quad \left. - (9c_2 + 32c_3 + 32c_4)g^2m^4(t - 2M^2)^2(2M^2 - t + \sigma) - 2(9c_2 + 32c_3 + 32c_4)g^2m^2\sigma^4 \right. \\
&\quad \left. + 4 \left[ 2c_4 - (9c_2 + 16c_3 + 14c_4)g^2 \right] (t - 2M^2 + \sigma)\sigma^4 \right\}, \\
D_{PCB}^{(4)-} &= \frac{1}{2304F^4\pi^2\sigma^3} \left\{ 32(2c_2 + 17c_3 - 19c_4)g^2m^2M^2(2M^2 - t)\sigma^2 \right. \\
&\quad \left. - 4 \left[ 144c_1 - 2c_3 - c_4 + 4(18c_1 + c_2 - c_3 - 7c_4)g^2 \right] t\sigma^4 \right. \\
&\quad \left. + 8 \left[ (72c_1 - 2c_2 - 6c_3 - 3c_4) + (36c_1 - 2c_2 + 9c_3 - 33c_4)g^2 \right] (t - 2M^2)\sigma^4 \right. \\
&\quad \left. - (9c_2 + 32c_3 + 32c_4)g^2m^2(t - 2M^2) \left[ 2m^2(2M^2 - t)(2M^2 - t + \sigma) + \sigma^2(4m^2 + \sigma) \right] \right. \\
&\quad \left. + \frac{4}{m^2} \left[ (34c_2 + 30c_3 - 3c_4) - (4c_2 + 15c_4)g^2 \right] \sigma^6 \right\}, \\
B_{PCB}^{(4)+} &= -\frac{m}{576f^4\pi^2\sigma^3} \left\{ 24c_4\sigma^4 + g^2 \left[ 32(2c_2 + 17c_3 - 19c_4)m^2M^2\sigma^2 + (67c_2 - 56c_3 + 96c_4)\sigma^4 \right] \right. \\
&\quad \left. + 2(9c_2 + 32c_3 + 32c_4)g^2m^4 \left[ 4M^4 + t^2 - t\sigma + 2\sigma^2 + M^2(-4t + 2\sigma) \right] \right\}, \\
B_{PCB}^{(4)-} &= \frac{m^3}{576f^4\pi^2\sigma^3} \left\{ \left[ 9c_2 + 32c_3 + 16c_4 - 2(9c_2 + 16c_3 - 28c_4)g^2 \right] \sigma^3 \right. \\
&\quad \left. + 2g^2m^2(9c_2 + 32c_3 + 32c_4)(2M^2 - t)(2M^2 - t + \sigma) \right\}. \quad (18)
\end{aligned}$$

Those PCB terms will be subtracted, namely absorbed by redefinition of the LECs, when performing the EOMS renormalization of the  $\pi N \rightarrow \pi N$  amplitude in section 2.5.

Before ending this subsection it may be worthwhile to mention that the PCB terms should be prevented from divergences induced by prefactors of the type

$$\frac{1}{\lambda(s, m^2, M^2)} \quad \text{and} \quad \frac{1}{\lambda(s, m^2, M^2) + s t}, \quad (19)$$

respectively, and so should the EOMS-renormalized amplitude be. The obstacle is first noted by Ref. [24], that the numerical analysis of the IR-renormalized amplitude encounters divergences at threshold  $s_{th} = (m + M)^2$  and at  $t = -\lambda(s, m^2, M^2)/s$ . Nevertheless, both the EOMS- and IR-renormalized amplitudes should possess good analytic properties at those  $s$  and  $t$  values, namely singularities caused by (19) are canceled by the numerators of the amplitudes. It can be easily seen from  $H_B(s)^{(i)} (i = 1, \dots, 6)$  and  $H_{13}^{(j)} (j = 1, 2)$  in Appendix C.1 that the prefactors are actually introduced by the standard Passarino-Veltman decomposition [34] of tensor integrals, which can be avoided by the new approach developed in Ref. [35].

Taking the tensor integral  $H_B^\mu$  for example, in Passarino-Veltman approach  $H_B^\mu$  is decomposed into

$$H_B^\mu = (p + \Sigma)^\mu H_B^{(1)} + (p - \Sigma)^\mu H_B^{(2)},$$

where the expressions for  $H_B^{(1)}$  and  $H_B^{(2)}$  refer to Eq. (C.5) and Eq. (C.6). On the other hand, following the approach in



Ref. [35],  $H_B^\mu$  is now decomposed into the new form

$$\begin{aligned} H_B^\mu &= P^\mu H_1 + \Sigma^\mu H_2, \\ H_1 &= \frac{\pi}{i} \int \frac{d^{d+2}k}{(2\pi)^{d+2}} \frac{1}{[M^2 - k^2] [m^2 - (P - k)^2] [m - (\Sigma - k)^2]}, \\ H_2 &= \frac{\pi}{i} \int \frac{d^{d+2}k}{(2\pi)^{d+2}} \frac{1}{[M^2 - k^2] [m^2 - (P - k)^2] [m - (\Sigma - k)^2]^2}, \end{aligned}$$

where  $H_1$  and  $H_2$  are already scalar loop integrals in dimension 6 momentum space, in other words, coefficient like  $1/\lambda(s, m^2, M^2)$  in standard Passarino-Veltman decomposition never occurs. Hence the threshold divergence introduced by  $1/\lambda(s, m^2, M^2)$  disappears, the same conclusion holds for the divergence at  $t = -\lambda(s, m^2, M^2)/s$  when considering  $H_{13}^\mu$ .

The new approach enables us to reduce the tensor integrals in the amplitude to scalar integrals defined in higher dimension momentum space, without confusion such as the divergence at threshold. If further regular parts of the scalar integrals are known, the PCB terms can be obtained in a new way. In Appendix D, the method proposed by Refs. [6, 50] is adopted to calculate the regular parts of the scalar integrals in dimension 4 space, those of the scalar integrals in higher dimension space can also be calculated term by term using the same method. With the aid of the regular parts, the PCB terms for  $H_1$  and  $H_2$  can be easily obtained, which are  $\frac{1}{32\pi^2 m^2}$  and  $\frac{1}{32\pi^2 m^2}$ , respectively. Using the relations  $H_B^{(1)} = \frac{1}{2}(H_1 + H_2)$  and  $H_B^{(2)} = \frac{1}{2}(H_1 - H_2)$ , one then gets the PCB terms for  $H_B^{(1)}$  and  $H_B^{(2)}$  in this new way, which are  $\frac{1}{32\pi^2 m^2}$  and 0 respectively. On the other hand, the PCB terms for  $H_B^{(1)}$  and  $H_B^{(2)}$  can also be obtained in the usual way adopted in the paper. One first replaces the scalar integrals in Eqs. C.5 and C.6 by their regular parts shown in Appendix D, then expands  $H_B^{(1)}$  and  $H_B^{(2)}$  in terms of  $\sigma, t, M_\pi$ . From the expanded expressions of  $H_B^{(1)}$  and  $H_B^{(2)}$ , one finds that the PCB terms for  $H_B^{(1)}$  and  $H_B^{(2)}$  are  $\frac{1}{32\pi^2 m^2}$  and 0, which are the same as the expressions obtained through the new way above. In this sense, the approach developed in Ref. [35] provides us a new way to obtain the PCB terms.

## 2.5. Renormalization

As an example, we will first show the renormalization of nucleon mass  $m_N$  as well as axial-vector coupling  $g_A$  to interpret the essence of EOMS scheme. Noticeably the expressions of  $m_N$  and  $g_A$  are also needed for replacing the corresponding bare quantities in the tree amplitude when performing numerical fits. Part of the results are already given in Ref. [36].

### 2.5.1. Nucleon mass and wave-function renormalization constant

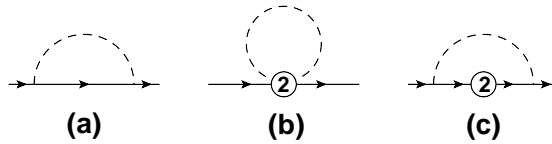


Figure 5: One-loop Feynman diagrams contributing to the self-energy of the nucleon up to  $O(p^4)$ . The vertex with circled ‘2’ stems from  $\mathcal{L}_{\pi N}^{(2)}$ .

As a simple example to illustrate the EOMS method, we evaluate the nucleon physical mass up to  $O(p^4)$ . The  $O(p^4)$  result of  $m_N$  in the EOMS scheme can also be found in Refs. [8, 37]. The one-loop Feynman diagrams are depicted in Fig. 5. A straightforward calculation leads to the primitive expression for the nucleon mass,

$$\begin{aligned} m_N &= m - 4c_1 M^2 - 2e_m M^4 - \frac{3mg^2}{2F^2} \left\{ \Delta_N - M^2 H(m^2) \right\} + \frac{3M^2}{F^2} \left\{ (2c_1 - c_3) - \frac{c_2}{d} \right\} \Delta_\pi \\ &\quad - \frac{3c_1 M^2 g^2}{F^2} \left\{ -2 \left[ \Delta_N - M^2 H(m^2) \right] + 4m^2 \left[ J_N(0) - M^2 H_A(0) \right] \right\}, \end{aligned}$$

where  $e_m = 8e_{38} + e_{115} + e_{116}$ . The second and third terms are tree contributions stemming from  $O(p^2)$  term involving  $c_1$  and  $O(p^4)$  term related to  $e_{38}$ ,  $e_{115}$  and  $e_{116}$ . The term with the first, second and third brace bracket represents the loop contribution from (a), (b) and (c) in Fig. 5, respectively. Definitions of all loop functions appeared here follow Appendix C.1. One can perform different renormalization schemes on the above expression of  $m_N$ , e.g. IR prescription, etc.. However, we proceed with the EOMS renormalization by first carrying out traditional  $\overline{\text{MS}} - 1$  subtraction, which gives

$$m_N = m^r - 4c_1^r M^2 - 2e_m^r M^4 - \frac{3mg^2}{2F^2} \left\{ \bar{\Delta}_N - M^2 \bar{H}(m^2) \right\} + \frac{3M^2}{F^2} \left\{ (2c_1 - c_3) - \frac{c_2}{d} \right\} \bar{\Delta}_\pi - \frac{3c_1 M^2 g^2}{F^2} \left\{ -2 \left[ \bar{\Delta}_N - M^2 \bar{H}(m^2) \right] + 4m^2 \left[ \bar{J}_N(0) - M^2 \bar{H}_A(0) \right] \right\}, \quad (20)$$

The bar over the loop function denotes the finite part of it, and the LEC with a subscript  $r$  means that it is a  $\overline{\text{MS}} - 1$  quantity<sup>7</sup>. The  $\overline{\text{MS}} - 1$  subtraction does nothing but shifts the divergencies in loop functions to the bare mass and LECs:

$$\begin{aligned} m^r &= m - \frac{3m^3 g^2 R}{32F^2}, \\ c_1^r &= c_1 + \frac{3g^2 m R}{128F^2 \pi^2} (1 - 12c_1 m), \\ e_m^r &= e_m + \frac{3R}{128F^2 \pi^2} \left[ -8c_1(1 + 3g^2) + c_2 + 4c_3 \right], \end{aligned}$$

where  $R = \frac{2}{d-4} + \gamma_E - 1 - \ln 4\pi$ . Since  $m_N$  is scale-independent, we now take the renormalization scale  $\mu = m$  in Eq. (C.4) for simplicity, and therefore  $\bar{\Delta}_N = 0$ . If the loop functions are replaced by their regular parts, one naively finds that the term  $\frac{3mM^2 g^2}{2F^2} \bar{H}(m^2)$  in Eq. (20) should be  $O(p^3)$ , but actually contributes an  $O(p^2)$  PCB term  $\frac{3mM^2 g^2}{32\pi^2 f^2}$ , and the same thing happens for the last term where a  $O(p^2)$  PCB term  $\frac{3c_1 m^2 M^2 g^2}{4F^2 \pi^2}$  occurs. Since they are polynomials, they can be absorbed by the LEC  $c_1^r$ ,

$$\tilde{c}_1 = c_1^r - \frac{3mg^2}{128F^2 \pi^2} (1 + 8c_1 m).$$

Finally, we get the expression for  $m_N$  in EOMS scheme, which takes the following form

$$m_N = \tilde{m} - 4\tilde{c}_1 M^2 - 2\tilde{e}_m M^4 + \frac{3mM^2 g^2}{2F^2} \bar{H}(m^2) + \frac{3M^2}{F^2} \left\{ (2c_1 - c_3) - \frac{c_2}{d} \right\} \bar{\Delta}_\pi - \frac{3c_1 M^2 g^2}{F^2} \left\{ 2M^2 \bar{H}(m^2) + 4m^2 \left[ \bar{J}_N(0) - M^2 \bar{H}_A(0) \right] \right\} - \frac{3mM^2 g^2}{32\pi^2 F^2} - \frac{3c_1 m^2 M^2 g^2}{4F^2 \pi^2}, \quad (21)$$

with  $\tilde{m} = m^r$ ,  $\tilde{e}_m = e_m^r$ , namely they are unaffected by the PCB terms.

We note that one can also carry out the mass renormalization by replacing  $m$  by  $m_4 = m - 4c_1 M^2 - 2e_m M^4$  in the nucleon propagator. In this case, the graph (c) in Fig. 5 is absent and automatically included in graph (a), and the result is

$$m_N = m - 4c_1 M^2 - 2e_m M^4 - \frac{3m_4 g^2}{2F^2} \left\{ \Delta_N - M^2 H(m_4^2) \right\} + \frac{3M^2}{F^2} \left\{ (2c_1 - c_3) - \frac{c_2}{d} \right\} \Delta_\pi, \quad (22)$$

while the wave-function renormalization constant of nucleon reads

$$Z_N = 1 - \frac{3g^2}{4F^2} \left\{ \Delta_\pi - 4m_4^2 M^2 \frac{\partial}{\partial s} H(s) \right\}_{\not{p}=m_N} - \frac{6c_2}{F^2 m_4} \frac{M^2}{d} \Delta_\pi. \quad (23)$$

Hereafter, the  $m_4$  related to loop contributions is always taken as  $m$  for short. Instead of Eq. (21), Eqs. (22) and (23) are adopted for the renormalization of the  $\pi$ -N scattering amplitude. Throughout this paper, we use this way to simplify our calculation for the reasons discussed in section 2.3.

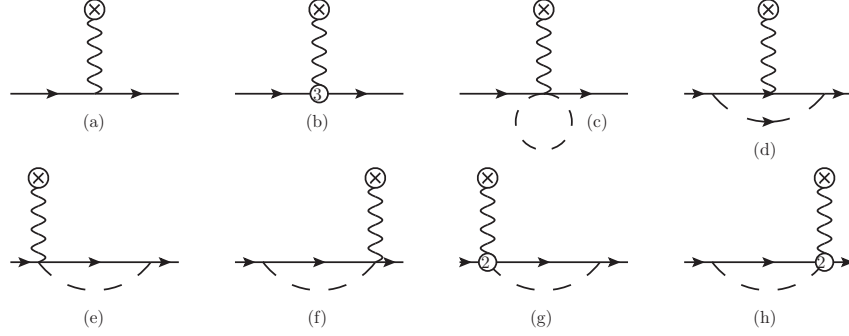


Figure 6: Diagrams contributing to the nucleon axial form factor  $G_A(t)$  up to  $O(p^4)$ . The wavy line with a circled cross at the end stands for the axial-vector current. The vertex with circled '2' and '3' stems from  $\mathcal{L}_{\pi N}^{(2)}$  and  $\mathcal{L}_{\pi N}^{(3)}$ , respectively.

### 2.5.2. Axial-vector coupling constant

The axial-vector current  $A^{\mu,a}(0)$  between one-nucleon states can be written as

$$\langle N(p') | A^{\mu,a}(0) | N(p) \rangle = \bar{u}(p') \left[ G_A(q^2) \gamma^\mu \gamma_5 + G_P(q^2) \frac{q^\mu}{2m} \gamma_5 \right] \frac{\tau^a}{2} u(p), \quad (24)$$

where  $q_\mu = p'_\mu - p_\mu$  and  $a$  is isospin index.  $G_A(q^2)$  is called the axial form factor and  $G_P(q^2)$  is the induced pseudoscalar form factor. The axial-vector coupling constant  $g_A$  is defined as

$$g_A = G_A(q^2 = 0). \quad (25)$$

Up to the  $O(p^4)$  diagrams in Fig. 6 are needed. A straightforward calculation leads to  $g_A$ :

$$\begin{aligned} g_A = & g + 4d_{16}M^2 - \frac{g^3m^2}{32F^2\pi^2} + \frac{g(4-g^2)}{2F^2}\Delta_N - \frac{g(2+g^2)}{2F^2}\Delta_\pi + \frac{g^3(2m^2+M^2)}{4F^2}J_N(0) \\ & - \frac{g(8-g^2)M^2}{4F^2}H(m^2) - \frac{g^2M^4}{4F^2}H_A(0) + \frac{3g^3m^2M^2}{F^2}\frac{\partial}{\partial s}H(s)\Big|_{p=m_N} - \frac{8c_4mg}{F^2}(\Delta_\pi - M^2H(m^2)) \\ & - \frac{2g}{mF^2}\left[c_2\left(4\frac{M^2}{d}\Delta_\pi + \frac{m^2}{d}\Delta_N - M^2H^{(2)}(m^2)\right) - 4(c_3+c_4)m^2H^{(2)}(m^2)\right], \end{aligned} \quad (26)$$

which agrees with Refs. [38, 39]<sup>8</sup>. Here, the EOMS renormalization procedure is similar to that for  $m_N$ . The bare  $g$  will be redefined as

$$\tilde{g} = g^r - \frac{g^3m^2}{16F^2\pi^2} - \frac{gm^3}{576F^2\pi^2}(9c_2 + 32c_3 + 32c_4), \quad g^r = g + \frac{gm^2R}{16F^2\pi^2}(2-g^2) - \frac{gm^3R}{96F^2\pi^2}(3c_2 + 8c_3 - 40c_4), \quad (27)$$

whereas the redefinition of the LEC  $d_{16}$  reads

$$\tilde{d}_{16} = d_{16}^r + \frac{mg}{288F\pi^2}(c_2 + 18c_3 - 18c_4), \quad d_{16}^r = d_{16} + \frac{R}{192F^2\pi^2}\left[3g(1-g^2) - mg(c_2 + 6c_3 - 18c_4)\right]. \quad (28)$$

The final expression for  $g_A$  is lengthy but rather straightforward to get with the help of Eqs. (27) and (28), so we do not present it here explicitly.

<sup>7</sup>Hereafter we denote the  $\overline{MS}$  - 1 and EOMS renormalized LECs with a superscript  $r$  (eg.  $c_1^r$ ) and overhead tilde (eg.  $\tilde{c}_1$ ) respectively.

<sup>8</sup>Though in Ref. [39] the mass insertion graphs are calculated directly, the comparison between our result and the one there is easy.

### 2.5.3. Full $\pi N \rightarrow \pi N$ amplitude

In order to present a full  $\pi N \rightarrow \pi N$  amplitude, we also need the formulae for  $M_\pi$  and  $F_\pi$ , and the corresponding  $Z$  factor for the pion. To  $O(p^4)$  level, these read

$$\begin{aligned} M_\pi^2 &= M^2 \left( 1 + 2\ell_3 \frac{M^2}{f^2} + \frac{1}{2f^2} \Delta_\pi \right), \\ F_\pi &= F \left[ 1 + \ell_4 \frac{M^2}{f^2} - \frac{1}{f^2} \Delta_\pi \right], \\ Z_\pi &= 1 + \frac{1}{f^2} \left[ \frac{2}{3} \Delta_\pi - 2\ell_4 M^2 \right]. \end{aligned} \quad (29)$$

All of them do not contain PCB terms from loop integrals, and hence can be treated traditionally.

Since all the necessary preparations are completed, we proceed with the renormalization of  $\pi N \rightarrow \pi N$  amplitude. Unlike the renormalization of  $m_N$  and  $g_A$ , it is hard to visualize the procedure of  $\pi N \rightarrow \pi N$  amplitude renormalization for its extremely lengthy expression. However, the essence is the same, that is to carry out renormalization procedure in two steps:  $\overline{\text{MS}} - 1$  renormalization and EOMS renormalization. Corresponding to the  $\overline{\text{MS}} - 1$  renormalization, those LECs appeared in the tree amplitudes are demanded to cancel the ultraviolet divergences and yield the so-called  $\overline{\text{MS}} - 1$  renormalized LECs,

$$c_i^r(\mu) = c_i - \frac{\gamma_i^c m R}{16\pi^2 F^2}, \quad d_j^r(\mu) = d_j - \frac{\gamma_j^d R}{16\pi^2 F^2}, \quad e_k^r(\mu) = e_k - \frac{\gamma_k^e R}{16\pi^2 F^2 m},$$

where details of  $\gamma_i^c, \gamma_j^d, \gamma_k^e$  can be found in Appendix E. To absorb the PCB terms (17) and (18),  $c_i^r(\mu)$  and  $d_j^r(\mu)$  are further redefined as

$$\tilde{c}_i = c_i^r - \frac{\delta_i^c m}{16\pi^2 F^2}, \quad \tilde{d}_j = d_j^r - \frac{\delta_j^d}{16\pi^2 F^2},$$

whereas  $e_k^r(\mu)$  remain the same, ie.  $\tilde{e}_k = e_k^r(\mu)$ , since the chiral order of PCB terms are lower than  $O(p^4)$ . Also  $\delta_i^c$  and  $\delta_j^d$  are specified in Appendix E. So far, we have already completed the renormalization of the  $\pi N \rightarrow \pi N$  amplitude in the EOMS scheme, the main feature of this method is characterized by additional EOMS subtractions, which distinguishes EOMS scheme from other prescriptions like IR and HB. We observe that an amplitude in EOMS scheme differs from the full covariant amplitude only by a polynomial of small quantities and hence owns the same analytical structure but possesses correct power counting. The validity of the  $\pi N \rightarrow \pi N$  description in EOMS scheme will also be judged by numerical fits to existing experimental data.

### 2.6. Partial wave expansions

We choose to perform fits to the partial wave phase shift data. The isospin decomposed amplitudes for  $\pi N$  scattering are

$$\begin{aligned} T^{I=\frac{1}{2}} &= T^+ + 2T^-, \\ T^{I=\frac{3}{2}} &= T^+ - T^-. \end{aligned} \quad (30)$$

The final partial wave amplitudes with isospin  $I$ , orbital momentum  $\ell$ , and total angular momentum  $J = \ell \pm \frac{1}{2}$  (denoted by  $\ell \pm$  concisely) take the form [1],

$$\begin{aligned} f_{\ell \pm}^I(s) &= \frac{1}{16\pi \sqrt{s}} \left\{ (E_p + m_N) \left[ A_\ell^I(s) + (\sqrt{s} - m_N) B_\ell^I(s) \right] \right. \\ &\quad \left. + (E_p - m_N) \left[ -A_{\ell \pm 1}^I(s) + (\sqrt{s} + m_N) B_{\ell \pm 1}^I(s) \right] \right\}, \end{aligned} \quad (31)$$

where

$$\begin{aligned} A_\ell^I(s) &= \int_{-1}^1 A^I(s, t) P_\ell(\cos \theta) d \cos \theta, \\ B_\ell^I(s) &= \int_{-1}^1 B^I(s, t) P_\ell(\cos \theta) d \cos \theta. \end{aligned}$$

Here  $E_p = \frac{s+m_N^2-M_\pi^2}{2\sqrt{s}}$  and  $\theta$  are the nucleon energy and scattering angle in center-of-mass system, respectively.  $P_\ell(\cos\theta)$  are the conventional Legendre polynomials. The angular variable  $\cos\theta$  relates to the Mandelstam variables via  $\cos\theta = 1 + \frac{2st}{\lambda(s, m_N^2, M_\pi^2)}$ , with  $\lambda(a, b, c) = a^2 + b^2 + c^2 - 2ab - 2bc - 2ac$  being the Källén function. As a straightforward consequence of unitarity of  $S$  matrix, one can further express the partial wave amplitudes by the phase shift  $\delta_{\ell\pm}^I$ ,

$$f_{\ell\pm}^I(s) = \frac{1}{2i|\vec{p}|} \left[ \exp(2i\delta_{\ell\pm}^I(s)) - 1 \right], \quad (32)$$

where  $\vec{p}$  is the 3-momentum of nucleon in the center-of-mass frame. Since the phase shift is real for elastic scattering, we follow Ref. [10] to related it with our perturbative computation of  $f_{\ell\pm}^I(s)$  via

$$\delta_{\ell\pm}^I(s) = \arctan \left\{ |\vec{p}| \operatorname{Re} f_{\ell\pm}^I(s) \right\}. \quad (33)$$

### 3. Phenomenological and numerical studies

In this section, we first perform fits to partial wave phase shift data near threshold to pin down the free LECs. In order to describe the partial wave phase shifts up to a higher energy region, we include explicitly the leading  $\Delta(1232)$  Born-term contribution and partially-included  $\Delta(1232)$  loop contribution. The contribution to the LECs from the  $\Delta(1232)$  resonance is also considered. We proceed with discussing the convergence of the chiral expansion of the resulting partial wave phase shift. The improvement of the fourth-order calculation compared with the third-order is shown. Finally, the deviation ( $\Delta_{GT}$ ) of Goldberger-Treiman relation and the pion-nucleon  $\sigma$  term  $\sigma_{\pi N}$  are discussed. The  $O(p^3)$  analyses are also included for the sake of comparison with the previous literature.

#### 3.1. Partial wave phase shift

To begin with, we first fit the partial waves at the  $O(p^3)$  level. We denote this fit by “Fit I- $O(p^3)$ ”. As input we use the phase shift data from Ref. [40], namely the current solution of George Washington University (GWU) group. Since the GWU group does not give data errors, we assign them with the method of Ref. [18],

$$\operatorname{err}(\delta) = \sqrt{e_s^2 + e_r^2 \delta^2}, \quad (34)$$

with the systematic error  $e_s = 0.1^\circ$  and the relative error  $e_r = 2\%$ . Throughout the numerical analyses, we employ  $g_A = 1.267$ ,  $F_\pi = 92.4$  MeV,  $m_N = 939$  MeV,  $M_\pi = 139$  MeV, and the renormalization scale  $\mu = m_N$ . There are 9 free LECs (or combinations of LECs) in total:  $c_{1-4}$ ,  $d_1 + d_2$ ,  $d_3$ ,  $d_5$ ,  $d_{14} - d_{15}$ ,  $d_{18}$ . All of them can be pinned down by fitting two S- and four P- partial waves. The fitting range is from threshold (1.078 GeV) up to 1.130 GeV in  $\sqrt{s}$ , and the interval between two data points is 4 MeV. The 2nd column in Table 1 collects our fit results at  $O(p^3)$  level. In column 3 of Table 1, we have also listed the results from Refs. [21] for comparison. We see that, in general, our fit results at  $O(p^3)$  level are in good agreement with those in Refs. [21], except for the  $d_5$  parameter. Especially, the  $d_{18}$ , related to  $\Delta_{GT}$ , is nearly the same.

The fourth-order analysis of  $\pi$ - $N$  scattering is denoted by “Fit I (a)- $O(p^4)$ ” in Table 2. There are 14 free LECs, which are four dimension two LECs:  $\hat{c}_1$ ,  $\hat{c}_2$ ,  $\hat{c}_3$ ,  $\hat{c}_4$ , five dimension three LECs:  $d_1 + d_2$ ,  $d_3$ ,  $d_5$ ,  $d_{14} - d_{15}$ ,  $d_{18}$ , and five dimension four LECs:  $e_{14}$ ,  $e_{15}$ ,  $e_{16}$ ,  $e_{17}$ ,  $e_{18}$ . Unlike the  $O(p^3)$  fit,  $d_{18}$  is now fixed at its  $O(p^3)$  fitted value, according to the discussion of  $\Delta_{GT}$  below in Sec. 3.4. The  $O(p^4)$  fit is performed up to 1.13 GeV too, and the results are shown in column 2 of Table 2. Also, we have taken the results of HB $\chi$ PT from Ref. [11] for comparison. Our results show improvements compared to Ref. [11]. First, from Table 2, one can observe that the  $\hat{c}_i$ ,  $d_j$  and  $e_k$  are mostly of natural size in EOMS scheme, but in HB results, especially Fit 2 in Table 1 of Ref. [11], some of the  $e_k$  come out fairly large. Second, our results seems to be more self-consistent. The  $\hat{c}_i$  change a lot when extending the  $O(p^3)$  analysis to the  $O(p^4)$  analysis in Ref. [11], while our  $\hat{c}_i$  change much more acceptably.

We plot both  $O(p^3)$  and  $O(p^4)$  fits in Fig. 7. Though fits are performed up  $\sqrt{s} = 1.13$  GeV, we plot up to 1.16 GeV. The conclusions made in Ref. [11] still hold: the  $P_{33}$  wave is slightly improved compared to the  $O(p^3)$  calculation, and the  $P_{11}$  partial wave are somewhat off above 1.14 GeV.

Note that the effect of unitarity is automatically included through the phase shift formula Eq. 33, which is discussed in Appendix F.

LEC	Fit I- $O(p^3)$	WI08 [21]	Fit II- $O(p^3)$	WI08 [23]
$c_1$	$-1.39 \pm 0.07$	$-1.50 \pm 0.06$	$-0.81 \pm 0.03$	$-1.00 \pm 0.04$
$c_2$	$4.01 \pm 0.09$	$3.74 \pm 0.09$	$1.46 \pm 0.09$	$1.01 \pm 0.04$
$c_3$	$-6.61 \pm 0.08$	$-6.63 \pm 0.08$	$-3.10 \pm 0.12$	$-3.04 \pm 0.02$
$c_4$	$3.92 \pm 0.04$	$3.68 \pm 0.05$	$2.35 \pm 0.06$	$2.02 \pm 0.01$
$d_1 + d_2$	$4.40 \pm 0.54$	$3.67 \pm 0.54$	$0.79 \pm 0.09$	$0.15 \pm 0.20$
$d_3$	$-3.02 \pm 0.51$	$-2.63 \pm 0.51$	$-0.47 \pm 0.05$	$-0.23 \pm 0.27$
$d_5$	$-0.62 \pm 0.13$	$-0.07 \pm 0.13$	$-0.17 \pm 0.04$	$0.47 \pm 0.07$
$d_{14} - d_{15}$	$-7.15 \pm 1.06$	$-6.80 \pm 1.07$	$-0.90 \pm 0.15$	$-0.5 \pm 0.5$
$d_{18}$	$-0.56 \pm 1.42$	$-0.50 \pm 1.43$	$-0.91 \pm 0.25$	$-0.2 \pm 0.8$
$h_A$	-	-	$2.82 \pm 0.04$	$2.87 \pm 0.04$
$\chi^2_{d.o.f}$	0.20	0.22	0.35	0.23

Table 1: LECs given by fit up to  $O(p^3)$ . Fit I is performed up to 1.13 GeV, while Fit II up to 1.20 GeV including the explicit  $\Delta(1232)$  contribution. For comparison, we provide the results from [21, 23]. The  $c_i$  and  $d_j$  have units  $\text{GeV}^{-1}$  and  $\text{GeV}^{-2}$  respectively, and  $h_A$  is dimensionless. In Fit II, the results correspond to  $c'_i$  and  $d'_j$  instead of  $c_i$  and  $d_j$ , respectively.

### 3.2. Contribution of $\Delta(1232)$

In this subsection, the effect of  $\Delta(1232)$  is explicitly included to describe the partial wave shift up to 1.20 GeV. Pascalutsa et al. discussed how to treat the  $\Delta(1232)$  as an explicit degree of freedom in covariant baryon chiral perturbation theory in Refs. [41–43]. The description of  $\Delta(1232)$  is subtle, because the conventional Rarita-Schwinger representation is a field with 16 components while only 8 of them are physical. However we adopt the *consistent* formulation here [42]. Additionally, we follow the so-called  $\delta$ -counting rule [41] which assigns an extra fractional suppression of  $O(p^{1/2})$  to the propagator of  $\Delta(1232)$ . Up to  $O(p^4)$  level, there are three typical  $\Delta(1232)$ -included Feynman diagrams of different order: Born-term of  $O(p^{3/2})$  and  $O(p^{5/2})$ , loop graphs of  $O(p^{7/2})$ . Refs. [20, 23] remarked that the contribution of Born-term of  $O(p^{5/2})$  is negligible. It is rather complicated to evaluate loop graphs of  $O(p^{7/2})$  in the EOMS scheme, since the loop diagrams involving both propagator of nucleon and  $\Delta(1232)$  will cause much more subtle PCB effects due to the heavy masses  $m_N$  and  $m_\Delta$ . So throughout this paper we consider the leading Born-term contribution of  $\Delta(1232)$ , whose expression can be found in Appendix A.1, together with partially-included  $\Delta$  loop contribution illustrated in Appendix A.2. The complete calculation with  $\Delta(1232)$  up to  $O(p^{7/2})$  is left as an open question. It is important to mention that the effect of the  $\Delta(1232)$  width is considered through the phase shift formula Eq. 33, which is amply discussed in Appendix G. Likewise, we will have the operators from Eqs. (8)–(10) but with couplings different from those in the  $\Delta$ -less effective field theory. We will mark the analogous coupling of the theory with  $\Delta(1232)$  with a prime, e.g.,  $c_i \rightarrow c'_i$ .

Corresponding to the two different fits performed in Sec. 3.1, we perform another two fits, “Fit II- $O(p^3)$ ” and “Fit II(a)- $O(p^4)$ ”, which explicitly include the  $\Delta(1232)$  contribution. The results are shown in the 4th column of Table 1 and Table 2, respectively. Taking into consideration the  $\Delta(1232)$  contribution to the LECs, the  $d_{18}$  is set free in both fits here. The leading Born-term contribution of  $\Delta(1232)$  is characterized by the  $N\Delta$  coupling  $h_A$ . The value of  $h_A = 2.90$  is determined from the Breit-Wigner width  $\Gamma_\Delta = 118\text{MeV}$ . In “Fit II(a)- $O(p^4)$ ”, we fix  $h_A = 2.90$ . However, for “Fit II- $O(p^3)$ ”,  $h_A$  is released as a free parameter, and its fitted value is 2.82. In Table 1, our result is found mostly compatible with those of Ref. [23]. We plot the  $\Delta$ -included  $O(p^3)$  and  $O(p^4)$  fits together in Fig.8 for the convenience of comparison. We find that, both  $O(p^3)$  and  $O(p^4)$  calculations with  $\Delta(1232)$  contribution give a reasonable description to data and the  $O(p^4)$  calculation improves the fit quality.

Note that we denote the  $O(p^4)$  fits with the notations: Fit I is  $\Delta$ -less and Fit II includes  $\Delta$ ; Fit (a) and Fit (b) are performed only with pion-nucleon phase shift data whereas Fit (b) has the  $c_i$  in  $\hat{c}_i$  fixed, and Fit (c) is performed with both phase shift data and lattice QCD data for  $m_N$ .

### 3.3. Convergence properties of partial wave phase shifts

We have made chiral expansions up to  $O(p^4)$ . It is necessary, at this stage, to check the convergence property of the chiral amplitudes. However, in the fits of Table 2 the  $O(p^2)$  parameters  $c_i$  mix with  $O(p^4)$  parameters  $e_i$ , so it is



LEC	Fit I(a)- $O(p^4)$	HB $\chi$ PT [11]	Fit II(a)- $O(p^4)$	Fit I(c)- $O(p^4)$	Fit II(c)- $O(p^4)$
$\hat{c}_1$	$-1.08 \pm 0.06$	$(-3.31, -0.27)$	$-1.03 \pm 0.03$	$-1.09 \pm 0.08$	$-0.95 \pm 0.05$
$\hat{c}_2$	$2.78 \pm 0.11$	$(0.13, 3.29)$	$0.50 \pm 0.04$	$2.44 \pm 0.05$	$0.10 \pm 0.06$
$\hat{c}_3$	$-5.26 \pm 0.14$	$(-10.37, -1.44)$	$-3.17 \pm 0.05$	$-5.05 \pm 0.22$	$-2.64 \pm 0.08$
$\hat{c}_4$	$2.43 \pm 0.19$	$(2.80, 3.53)$	$0.79 \pm 0.03$	$2.43 \pm 0.19$	$0.80 \pm 0.03$
$d_1 + d_2$	$6.29 \pm 0.12$	$(4.45, 5.68)$	$2.99 \pm 0.05$	$6.18 \pm 0.11$	$2.93 \pm 0.05$
$d_3$	$-6.87 \pm 0.16$	$(-4.91, -2.96)$	$-5.04 \pm 0.05$	$-6.87 \pm 0.15$	$-4.90 \pm 0.04$
$d_5$	$0.51 \pm 0.11$	$(-0.95, -0.09)$	$1.32 \pm 0.04$	$0.55 \pm 0.11$	$1.24 \pm 0.03$
$d_{14} - d_{15}$	$-12.09 \pm 0.24$	$(-11.14, -7.02)$	$-5.61 \pm 0.09$	$-11.94 \pm 0.23$	$-5.58 \pm 0.09$
$d_{18}$	$-0.56^*$	$(-1.53, -0.85)$	$1.14 \pm 0.20$	$-0.56^*$	$1.64 \pm 0.17$
$e_{14}$	$3.69 \pm 0.36$	$(-4.68, 7.83)$	$-4.53 \pm 0.09$	$-1.80 \pm 0.33$	$-8.22 \pm 0.08$
$e_{15}$	$-14.99 \pm 0.55$	$(-18.41, 9.72)$	$5.05 \pm 0.13$	$-5.41 \pm 0.57$	$10.52 \pm 0.12$
$e_{16}$	$7.35 \pm 0.35$	$(6.42, 7.79)$	$-0.31 \pm 0.07$	$4.34 \pm 0.28$	$-1.50 \pm 0.05$
$e_{17}$	$-2.29 \pm 1.34$	$(-17.79, 14.88)$	$16.98 \pm 0.15$	$-2.23 \pm 1.42$	$15.70 \pm 0.15$
$e_{18}$	$6.07 \pm 1.18$	$(-9.15, 19.66)$	$-10.99 \pm 0.12$	$6.00 \pm 1.26$	$-9.87 \pm 0.12$
$h_A$	-	-	$2.90^*$	-	$2.90^*$
$e_1$	-	-	-	$15.48 \pm 0.30$	$16.70 \pm 0.27$
$m$	-	-	-	$0.88 \pm 0.02$	$0.89 \pm 0.03$
$\chi^2_{d.o.f}$	0.04	$(0.008, 0.44)$	0.23	0.51	0.36

Table 2: LECs given by fit up to  $O(p^4)$ . Fit I(a) and Fit II(a) are performed with phase shift data, while Fit I(c) and Fit II(c) with both phase shift data and QCD lattice data (see section 3.5). Fit I(a) and Fit I(c) are performed up to 1.13 GeV, while Fit II(a) and Fit II(c) up to 1.20 GeV including the explicit  $\Delta(1232)$  contribution. In Fit II(a) and Fit II(c), the results correspond to  $\hat{c}'_i$ ,  $d'_j$  and  $e'_k$  instead of  $\hat{c}_i$ ,  $d_j$  and  $e_k$ , respectively. For comparison, we provide the results from [11]. The  $c_i$ ,  $d_j$  and  $e_k$  have, respectively, units of  $\text{GeV}^{-1}$ ,  $\text{GeV}^{-2}$  and  $\text{GeV}^{-3}$ , and  $h_A$  is dimensionless. The \* denotes an input quantity.

not suitable for testing the convergence of the chiral expansion. To overcome the problem, here we follow the strategy of Ref. [11] to redo the fits. That is, we fix  $c_{1-4}$  in  $\hat{c}_{1-4}$  of Eq. (16) with their corresponding fit values at  $O(p^3)$  level given in Table 1. In other words, we perform fits with four dimension-4 combinations:  $e_{22} - 4e_{38}$  (in  $\hat{c}_1$ ),  $e_{20} + e_{35}$  (in  $\hat{c}_2$ ),  $2e_{19} - e_{22} - e_{36}$  (in  $\hat{c}_3$ ),  $2e_{21} - e_{37}$  (in  $\hat{c}_4$ ), instead of  $\hat{c}_{1-4}$ . For clarity, we will denote the modified  $O(p^4)$  fits discussed here by “Fit I(b)- $O(p^4)$ ” and “Fit II(b)- $O(p^4)$ ”, respectively. In this case, the contributions from different orders are separated, so we can study the convergence of the amplitude. The resulting values for the LECs are shown in Table 3.

Comparing “Fit I(b)- $O(p^4)$ ” results with those from Ref.[11], which are summed as intervals listed in the third column of Table 3, it is found, however, that most of our fitted  $d_j$  and  $e_k$  do not locate inside the intervals. The main reason might be that our primitive values for  $c_{2-4}$  as input are not in the corresponding intervals (see Table 3), which cause the incomparability since a small variation of  $c_i$  may lead to big changes of the higher order LECs,  $d_j$  and  $e_k$ , though both our fit and that of Ref. [11] maintain a good convergence property.

The convergence can be visualized by plotting contributions from  $O(p)$ ,  $O(p^2)$ ,  $O(p^3)$ ,  $O(p^4)$  separately, and the sum of them in Fig. 9. Note that we plot up to 1.20 GeV, though fit only up to 1.13 GeV. One can observe that the  $O(p^4)$  contributions (cyan dashed-dotted lines in Fig. 9) are in general small for all the partial waves below 1.13 GeV. The  $O(p^3)$  contributions (magenta dotted lines) are mostly larger than  $O(p)$  contributions (green dashed lines), with the exception of the  $S_{11}$  and  $P_{33}$  partial waves. However, there exist cancellations between the  $O(p^2)$  (blue shorted dashed lines) and  $O(p^3)$  contributions. The red solid lines represent the total contribution up to  $O(p^4)$ . They describe the existing partial wave data below 1.13 GeV very well. After all, the convergence property of the fourth-order calculation is reasonable, while the third-order calculation is not satisfactory as pointed out by Ref. [23].

In Fig. 10 we include the  $\Delta$  contribution and plot the contribution from  $\Delta(1232)$  together with the contributions from  $O(p)$ ,  $O(p^2)$ ,  $O(p^3)$ ,  $O(p^4)$ , and the sum of them. From the yellow short dash-dotted lines in Fig. 10, we can observe that  $\Delta(1232)$  mainly contributes to  $P_{33}$ -wave while the contribution for other channels is nonzero but very small. On the other hand, the chiral series are in general well convergent near threshold almost for all the partial

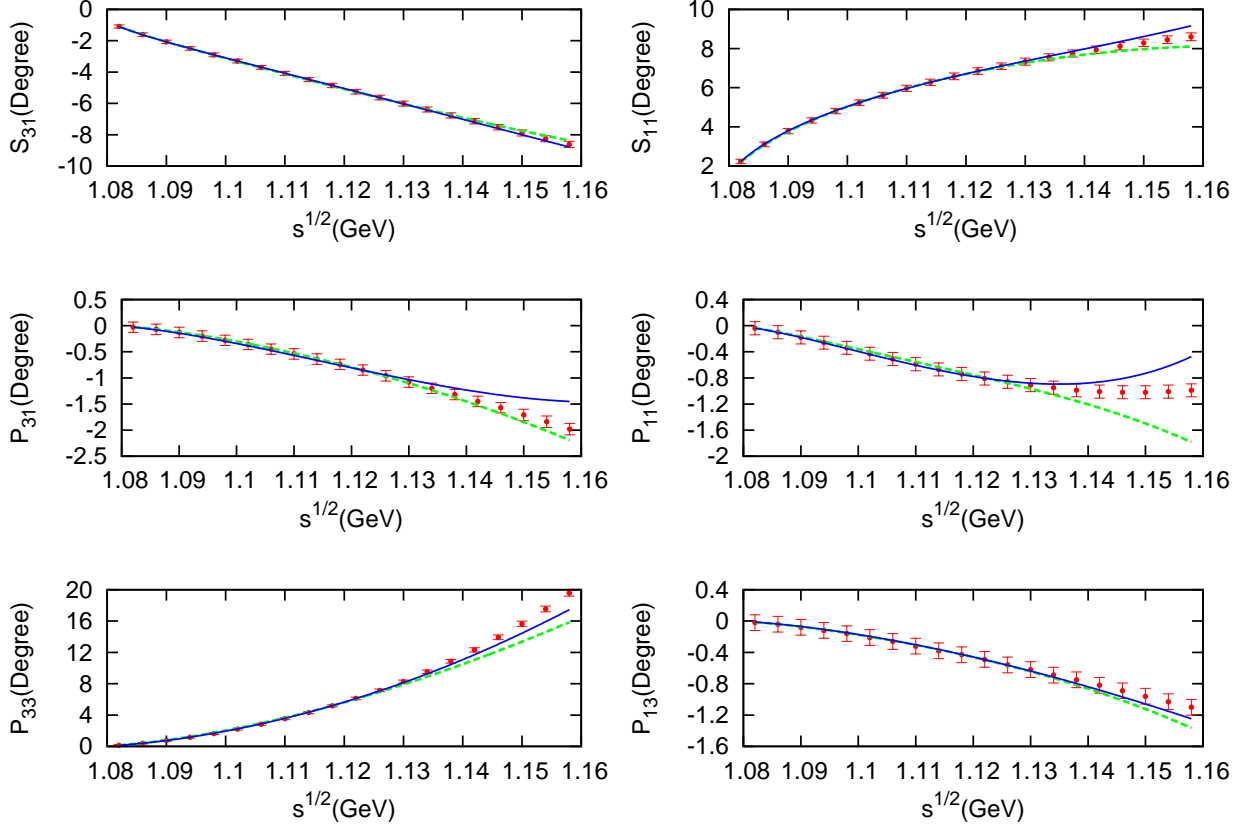


Figure 7: (Color online) Fit up to 1.13 GeV. The fourth- and third-order fits are presented by the blue solid and green dash lines respectively. Results of Fit I(a)- $O(p^4)$  in Table 2 and Fit I- $O(p^3)$  in Table 1 are adopted for plotting.

waves. However when increasing the energy far above the threshold, the convergence becomes worse. Especially, we can see from the Fig. 10 that the higher chiral order contributions grow much more rapidly than the lower chiral order contributions as the energy increases. This indicates that the chiral perturbation expansion breaks down in the large energy region and stops being valid.

#### 3.4. Goldberger-Treiman relation

The Goldberger-Treiman (GT) relation [44] is a straightforward result of PCAC and chiral symmetry, which connects the  $\pi$ - $N$  pseudoscalar (Yukawa) coupling constant  $g_{\pi N}$  with the axial vector coupling of nucleon  $g_A$ . Here its correction up to and including terms of  $O(p^3)$  is obtained. In our discussion below, one can observe that the  $O(p^3)$  correction, denoted by  $\Delta_{loops}^{(3)}$ , is negligible compared with the  $O(p^2)$  correction.

The GT relation reads

$$g_{\pi N} = \frac{g_A m_N}{F_\pi} (1 + \Delta_{GT}) , \quad (35)$$

where  $\Delta_{GT}$  represents the correction which can be divided into three parts,

$$\Delta_{GT} = -\frac{2\tilde{d}_{18}}{g_A} M_\pi^2 + \Delta_{loop}^{(2)} + \Delta_{loop}^{(3)} , \quad (36)$$



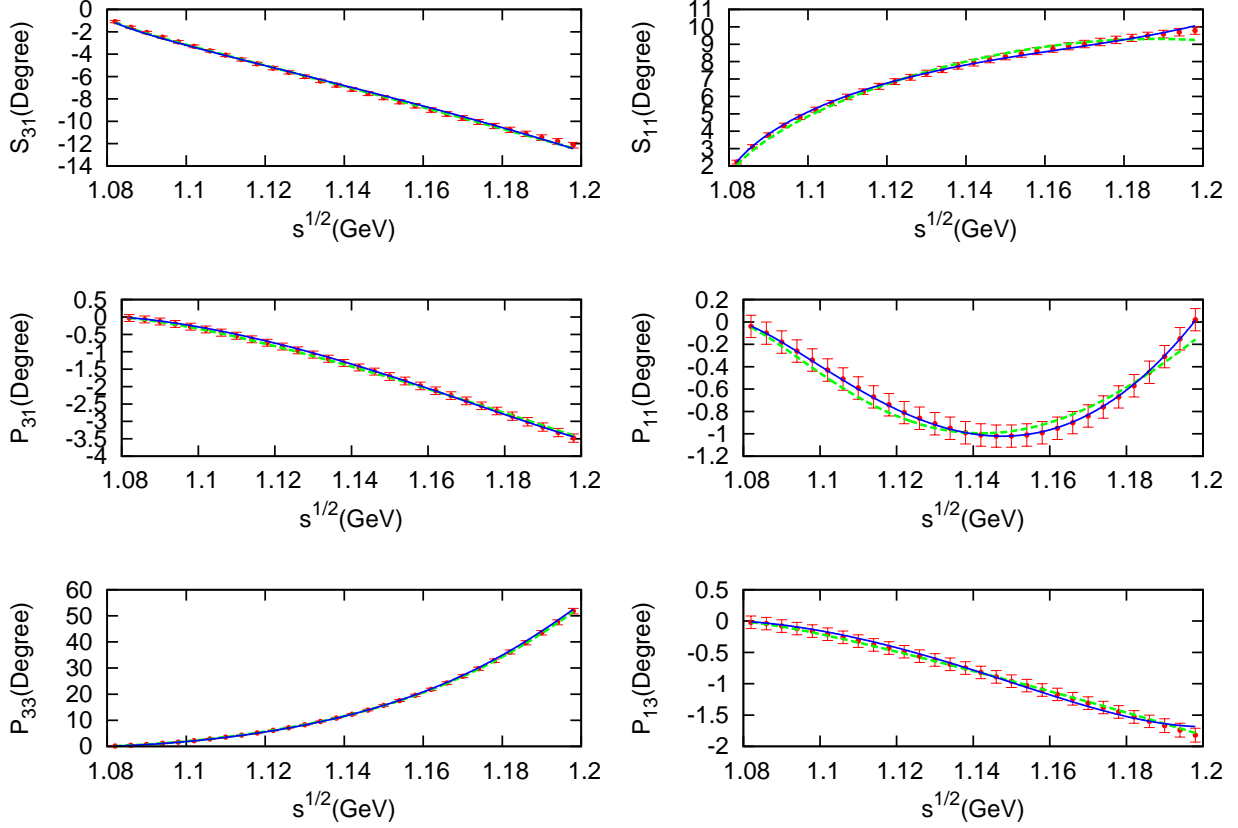


Figure 8: (Color online) Fit up to 1.20 GeV. The fourth- and third-order fits are presented by the blue solid and green dash lines respectively. Results of Fit II(a)- $O(p^4)$  in Table 2 and Fit II- $O(p^3)$  in Table 1 are adopted for plotting.

with

$$\Delta_{loops}^{(2)} = -\frac{m_N^2 g_A^2}{f_\pi^2} \left\{ \bar{H}^{(1)}(m_N^2) + \left( M_\pi^2 \bar{H}_A(M_\pi^2) - \bar{J}_N(M_\pi^2) \right) - \left( M_\pi^2 \bar{H}_A(0) - \bar{J}_N(0) \right) + 2\bar{H}_A^{(2)}(0) \right\}, \quad (37)$$

$$\Delta_{loops}^{(3)} = \frac{4\tilde{c}_1 M_\pi^2}{m_N F_\pi^2} \left( \bar{\Delta}_\pi - 2m_N^2 \bar{H}^{(1)}(m_N^2) \right) + \frac{\tilde{c}_2}{2F_\pi^2 m_N^3} \left[ 2(2m_N^2 - M_\pi^2) M_\pi^2 \bar{H}^{(2)}(m_N) - M_\pi^2 (m_N^2 - \frac{M_\pi^2}{2}) \bar{H}^{(1)}(m_N^2) + M_\pi^2 \bar{\Delta}_\pi^{(2)} \right. \\ \left. + \frac{1}{2} M_\pi^4 \bar{\Delta}_\pi - \frac{1}{2} M_\pi^6 \left( \bar{H}(m_N^2) - \bar{H}^{(1)}(m_N^2) \right) \right] + \frac{2(\tilde{c}_3 + \tilde{c}_4) m_N M_\pi^2}{F_\pi^2} \bar{H}^{(3)}(m_N^2) - \frac{(\tilde{c}_2 - \tilde{c}_3 - \tilde{c}_4) m_N M_\pi^2}{72 F_\pi^2 \pi^2}. \quad (38)$$

The first term related to  $\tilde{d}_{18}$  is  $O(p^2)$  and generates the main contribution to  $\Delta_{GT}$ , e.g. 1.71% for Fit I- $O(p^3)$ . In contrast, though  $\Delta_{loops}^{(2)}$  is also  $O(p^2)$ , it contributes a much smaller value,  $\Delta_{loops}^{(2)} \sim 0.36\%$ . In addition, we can see from Eq. (37) that its contribution is independent of the LECs. The last term in Eq. (38) is employed to cancel the PCB terms generated by the terms before it. According to the naive power counting rule  $\Delta_{loops}^{(3)}$  should be  $O(p^3)$ , but actually it possesses a chiral order higher than  $O(p^4)$  and including  $O(p^4)$ . This can be easily observed if we reduce all the tensor integrals in Eq. (38) to scalar integrals and a common prefactor  $M_\pi^4$  of order four will show up. It can be estimated by evaluating the loop integrals numerically, which leads to  $\Delta_{loops}^{(3)} = [-7.07\tilde{c}_1 + 1.79\tilde{c}_2 - 2.30(\tilde{c}_3 + \tilde{c}_4)] \times 10^{-4}$ . Because the fitted  $\hat{c}_{1-4}$  in Fit I- $O(p^4)$  are combinations of dimension 2 and 4 LECs, we prefer to bring the corresponding Fit I- $O(p^3)$  results in Table 1 into  $\Delta_{loop}^{(3)}$  to estimate its value, which gives  $\Delta_{loop}^{(3)} \cong 0.23\%$ .

LEC	Fit I(b)- $O(p^4)$	HB $\chi$ PT	Fit II(b)- $O(p^4)$
$c_1$	$-1.39^*$	$(-1.47, -1.21)$	$-0.81^*$
$c_2$	$4.01^*$	$(3.13, 3.29)$	$1.46^*$
$c_3$	$-6.61^*$	$(-6.14, -5.85)$	$-3.10^*$
$c_4$	$3.92^*$	$(3.47, 3.50)$	$2.35^*$
$d_1 + d_2$	$7.39 \pm 0.11$	$(4.90, 5.32)$	$3.18 \pm 0.05$
$d_3$	$-8.04 \pm 0.13$	$(-4.37, -3.61)$	$-4.75 \pm 0.04$
$d_5$	$0.62 \pm 0.11$	$(-1.03, -0.13)$	$1.11 \pm 0.03$
$d_{14} - d_{15}$	$-13.90 \pm 0.20$	$(-9.31, -8.70)$	$-5.82 \pm 0.09$
$d_{18}$	$-0.56^*$	$(-1.49, -0.84)$	$-0.15 \pm 0.17$
$e_{14}$	$3.25 \pm 0.37$	$(2.33, 4.19)$	$-9.78 \pm 0.08$
$e_{15}$	$-14.50 \pm 0.55$	$(-3.33, 4.54)$	$15.29 \pm 0.12$
$e_{16}$	$7.65 \pm 0.35$	$(2.74, 5.69)$	$-2.76 \pm 0.07$
$e_{17}$	$8.21 \pm 1.34$	$(5.14, 7.20)$	$18.35 \pm 0.14$
$e_{18}$	$-0.79 \pm 1.19$	$(-3.36, -1.27)$	$-11.58 \pm 0.11$
$e_{22} - 4e_{38}$	$-8.19 \pm 1.79$	$(7.38, 27.72)$	$10.29 \pm 0.82$
$e_{20} + e_{35}$	$-12.86 \pm 0.83$	$(-17.35, -10.49)$	$-13.12 \pm 0.28$
$2e_{19} - e_{22} - e_{36}$	$18.18 \pm 1.72$	$(-25.12, -1.49)$	$0.83 \pm 0.55$
$2e_{21} - e_{37}$	$-32.74 \pm 3.40$	$(-7.12, -1.66)$	$-25.46 \pm 0.48$
$h_A$	-	-	$2.90^*$
$\chi^2_{d.o.f}$	0.03	$(0.14, 0.58)$	0.11

Table 3: LECs given by fit up to  $O(p^4)$ . Fit I(b) and Fit II(b) are performed with  $c_i$  in  $\hat{c}_i$  are fixed at the corresponding  $O(p^3)$  fit values shown in Table 1, see the explanation in the text. Fit I(b) is performed up to 1.13GeV, while Fit II(b) up to 1.20GeV including explicit  $\Delta(1232)$  contribution. In Fit II(b), the results correspond to  $\hat{c}'_i$ ,  $d'_j$  and  $e'_k$  instead of  $\hat{c}_i$ ,  $d_j$  and  $e_k$ , respectively. For comparison, we provide the results from [11]. The  $c_i$ ,  $d_j$  and  $e_k$  have, respectively, units of  $\text{GeV}^{-1}$ ,  $\text{GeV}^{-2}$  and  $\text{GeV}^{-3}$ , and  $h_A$  is dimensionless. The \* denotes an input quantity.

In conclusion, the correction to GT relation can be rewritten much more explicitly as

$$\Delta_{GT} = \left\{ -3.05\tilde{d}_{18} + 0.36 + [-7.07\tilde{c}_1 + 1.79\tilde{c}_2 - 2.30(\tilde{c}_3 + \tilde{c}_4)] \times 10^{-2} \right\} \times 10^{-2}, \quad (39)$$

The first two terms contribute about 2.07%, while the last term stands for the next order contribution which is 0.23%. This indicates good convergence of the  $\Delta_{GT}$ . Practically, the calculation of  $\Delta_{GT}$  to at  $O(p^2)$  is sufficient, since  $\Delta_{GT}^{(3)}$  is negligible. Hence in our  $O(p^4)$  fits without explicit  $\Delta(1232)$ , the parameter  $d_{18}$  is fixed at the  $O(p^3)$ -fit value.

### 3.5. pion-nucleon $\sigma$ term: $\sigma_{\pi N}$

In what follows, an explicit expression for  $\sigma_{\pi N}$  up to  $O(p^4)$  is introduced. Then fits are performed both including  $\pi$ -N phase shift data and QCD lattice data to fix the unknown LECs related to  $\sigma_{\pi N}$ . Finally, the fit values are used to predict  $\sigma_{\pi N}$ :  $\sigma_{\pi N} = 52 \pm 7$  MeV for Fit I (c) without  $\Delta(1232)$  and  $\sigma_{\pi N} = 45 \pm 6$  MeV for Fit II (c) with the explicit  $\Delta(1232)$  contribution.

The sigma term is a quantity of great physical importance to understand the composition of the nucleon mass. It is defined as the matrix element of the explicit chiral symmetry breaking part of the QCD Lagrangian situated between the nucleon states at zero momentum transfer,

$$\sigma_{\pi N} = \sum_{q=u,d} m_q \frac{dm_N}{dm_q} = \langle N | m_u \bar{u}u + m_d \bar{d}d | N \rangle. \quad (40)$$

Using the Gell-Mann-Oakes-Renner relation  $M_\pi^2 = B_0(m_u + m_d)$ , the above equation becomes

$$\sigma_{\pi N} = M_\pi^2 \frac{\partial m_N}{\partial M_\pi^2}, \quad (41)$$

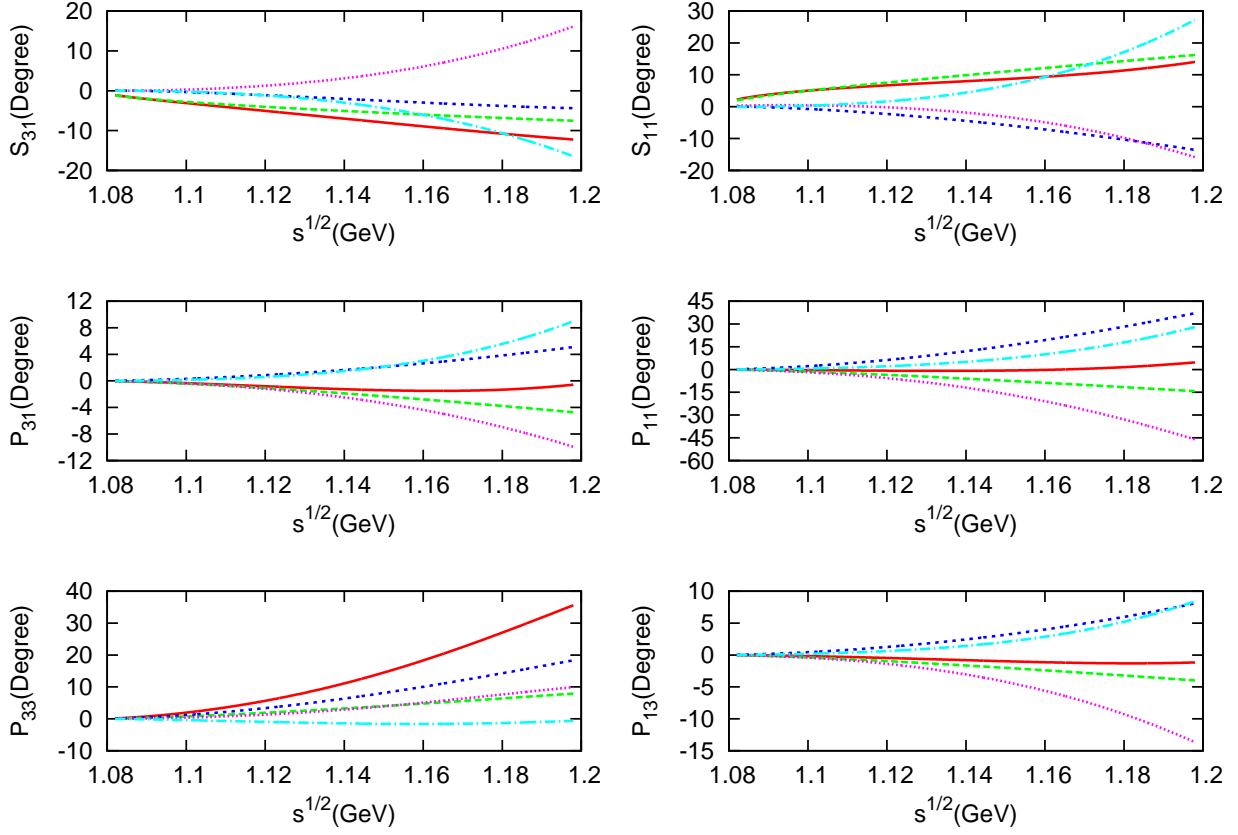


Figure 9: (Color online) Convergence properties of the chiral series. The results of Fit I(b) in Table 3 are adopted for plotting. The dashed (green), short-dashed (blue), dotted (magenta), dash-dotted (cyan), and solid (red) line represents  $O(p^1)$ ,  $O(p^2)$ ,  $O(p^3)$ ,  $O(p^4)$ , and total contribution, respectively.

where  $m_N$  takes the following explicit form derived by Eq. (21),

$$\begin{aligned}
 m_N = & m - 4\tilde{c}_1 M_\pi^2 + \tilde{e}_1 M_\pi^4 - \frac{3m g_A^2 M_\pi^2}{32\pi^2 F_\pi^2} \left\{ \frac{M_\pi}{m^2} \sqrt{4m^2 - M_\pi^2} \arccos \frac{M_\pi}{2m} + \frac{M_\pi^2}{2m^2} \ln \frac{M_\pi^2}{m^2} \right\} + \frac{3\tilde{c}_2 M_\pi^4}{128\pi^2 F_\pi^2} \\
 & + \frac{M_\pi^4}{16\pi^2 F_\pi^2} \left\{ 8\tilde{c}_1 - 3\tilde{c}_3 - \frac{3}{4}\tilde{c}_2 \right\} \ln \frac{M_\pi^2}{m^2} - \frac{3\tilde{c}_1 g_A^2 M_\pi^4}{8\pi^2 F_\pi^2} \left\{ 1 - \frac{M_\pi^2 - 2m^2}{2m^2} \ln \frac{M_\pi^2}{m^2} + \frac{(M_\pi^2 - 2m^2) M_\pi}{m^2 \sqrt{4m^2 - M_\pi^2}} \arccos \frac{M_\pi}{2m} \right\}, \quad (42)
 \end{aligned}$$

here  $m$  is the nucleon mass in the chiral limit and  $\tilde{e}_1 \equiv -2(4e_{22} - 8e_{38} + e_{115} + e_{116} - 4\tilde{c}_1 \tilde{\ell}_3 / F_\pi^2)$ . Actually,  $\tilde{c}_1$  is the EOMS renormalized quantity for  $\hat{c}_1 = c_1 - 2M^2(e_{22} - 4e_{38})$ . All the quantities except  $m$  on the right-hand side of Eq. (42) are substituted by the physical ones.  $\sigma_{\pi N}$  is obtained straightforwardly,

$$\begin{aligned}
 \sigma_{\pi N} = & -4\tilde{c}_1 M_\pi^2 + \tilde{e}_1 M_\pi^4 - \frac{3g_A^2 M_\pi^3}{16\pi^2 F_\pi^2 m} \left\{ \frac{3m^2 - M_\pi^2}{\sqrt{4m^2 - M_\pi^2}} \arccos \frac{M_\pi}{2m} + M_\pi \ln \frac{M_\pi}{m} \right\} + \frac{M_\pi^4}{16\pi^2 F_\pi^2} \left\{ 8\tilde{c}_1 - 3\tilde{c}_3 - \frac{3}{4}\tilde{c}_2 \right\} \left( 4 \ln \frac{M_\pi^2}{m^2} + 1 \right) \\
 & + \frac{3\tilde{c}_2 M_\pi^4}{64\pi^2 F_\pi^2} - \frac{3\tilde{c}_1 g_A^2 M_\pi^4}{8\pi^2 F_\pi^2} \left\{ \frac{4m^2 - 3M_\pi^2}{m^2} \ln \frac{M_\pi}{m} + \frac{12m^2 - 2M_\pi^2}{4m^2 - M_\pi^2} + \frac{26m^2 M_\pi^3 - 60m^4 M_\pi - 3M_\pi^5}{m^2(4m^2 - M_\pi^2)^{\frac{3}{2}}} \arccos \frac{M_\pi}{2m} \right\}. \quad (43)
 \end{aligned}$$

At  $O(p^3)$   $\sigma_{\pi N}$  can be determined by the value of  $c_1$ . In Ref. [20], through an analysis on  $\pi$ -N scattering partial wave phase shift data using the EOMS-B $\chi$ PT, it predicts  $\sigma_{\pi N} = 59 \pm 7$  MeV. At  $O(p^4)$   $\sigma_{\pi N}$  in Eq. (43) has the unknown

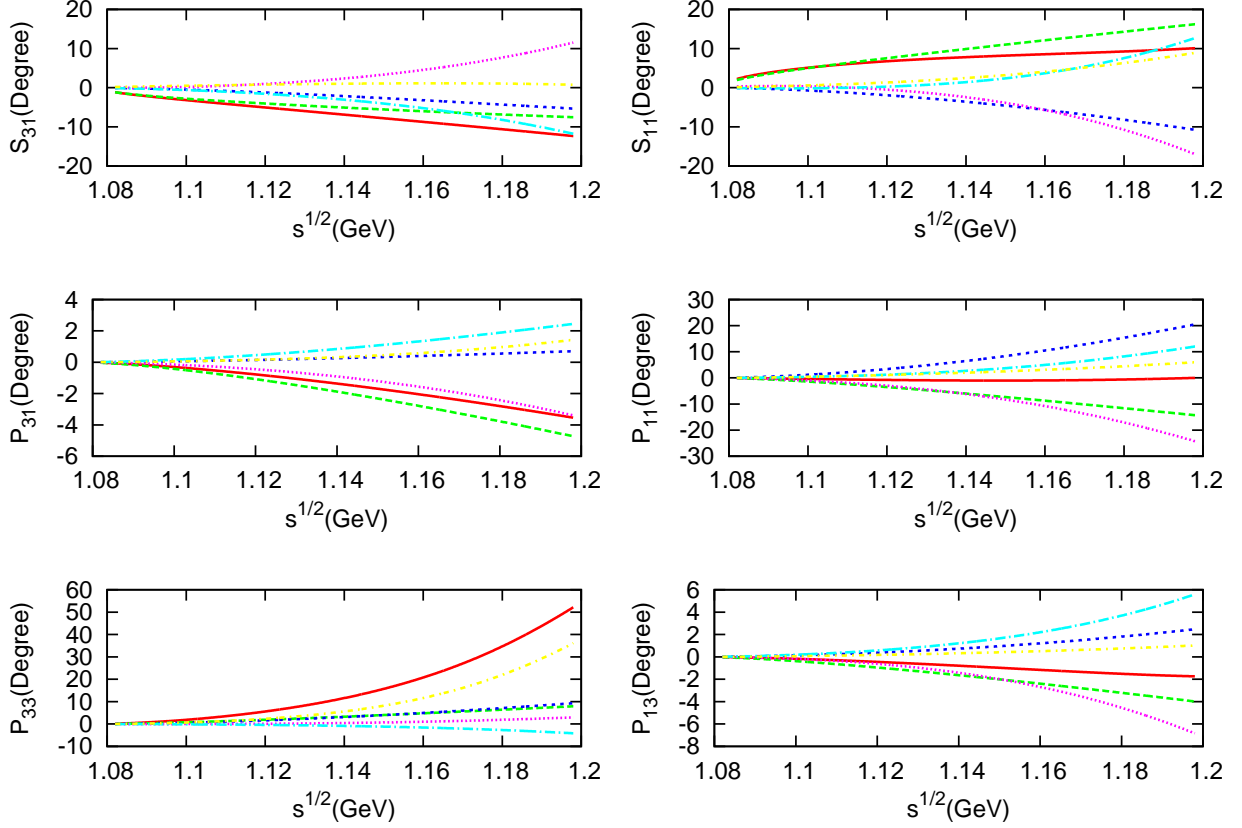


Figure 10: (Color online) Convergence properties of the chiral series with explicit  $\Delta(1232)$ . The results of Fit II(b) in Table 3 are adopted for plotting. The dashed (green), short-dashed (blue), dotted (magenta), dash-dotted (cyan), short-dash-dotted (yellow) and solid (red) line represents respectively  $O(p^1)$ ,  $O(p^2)$ ,  $O(p^3)$ ,  $O(p^4)$ ,  $\Delta(1232)$  and total contribution.

coupling constants combination  $e_1$  which does not appear in the  $\pi$ -N scattering amplitude. However, recently the lattice QCD simulations have gotten many data on the quark mass dependence of the nucleon mass, which enables us to fix  $e_1$  as well as  $c_1$ . Taking only the lattice QCD data into consideration, chiral effective field theory have been used to predict  $\sigma_{\pi N}$  up to  $O(p^4)$  [29, 31]. In the current paper, fits are performed both including the  $\pi$ -N scattering partial wave phase shift data and lattice QCD data. In our fits, lattice QCD data are taken from PACS-CS [45], LHPC [46], HSC [47], QCDSF-UKQCD [48] and NPLQCD [49] collaborations. Following the strategy of Ref. [29], in order to minimize uncertainties of finite volume effects we only use the data with  $M_\pi L > 4$ , and we also only choose those with  $M_\pi^2 < 0.25 \text{ GeV}^2$ . So there are only 11 lattice data points which meet the requirements. They are denoted with stars in the tables of the Appendix A in [29]. Note that the physical nucleon mass is included in the fits as a constraint. Compared with the previous fits to partial wave phase shift data, two additional fit parameters:  $m$  and  $e_1$  are included. The fit results are listed in Table 2, where in Fit II(c) the leading  $\Delta$ -exchange Born term and the partially-included  $\Delta$  loop contribution (see Appendix A.2) are considered whereas Fit I(c) does not. The predicted nucleon mass as a function of pion mass is plotted in Fig. 11.

From Table 2, we find that most fit parameters in Fit I(c) and Fit II(c) change little compared with Fit I(a) and Fit II(a) in Table 2, respectively. The prediction for  $\sigma_{\pi N}$  are:  $\sigma_{\pi N} = 52 \pm 7 \text{ MeV}$  for Fit I(c) and  $\sigma_{\pi N} = 45 \pm 6 \text{ MeV}$  for Fit II(c). Our result  $\sigma_{\pi N} = 52 \pm 7 \text{ MeV}$  is smaller than the result obtained from the fit to the  $\pi$ -N scattering partial wave phase shift data up to  $O(p^3)$  given in Ref. [20]:  $\sigma_{\pi N} = 59 \pm 7 \text{ MeV}$ . We improve our determination of  $\sigma_{\pi N}$  in two ways. On one hand, the fourth-order correction to  $\sigma_{\pi N}$  is obtained. On the other hand, to our knowledge, this is the first

attempt to treat the  $\pi$ -N scattering data and lattice QCD data together using the EOMS-B $\chi$ PT up to  $O(p^4)$ , and this may constrain the value of the sigma term better. The result:  $\sigma_{\pi N} = 45 \pm 6$  MeV agrees well with the recent analysis on lattice QCD data using EOMS-B $\chi$ PT up to  $O(p^4)$  [29], which gives  $\sigma_{\pi N} = 43(1)(6)$  MeV. However, because the exact  $\Delta$ -included loop graphs are not considered,  $\sigma_{\pi N} = 45 \pm 6$  MeV can still be improved in future.

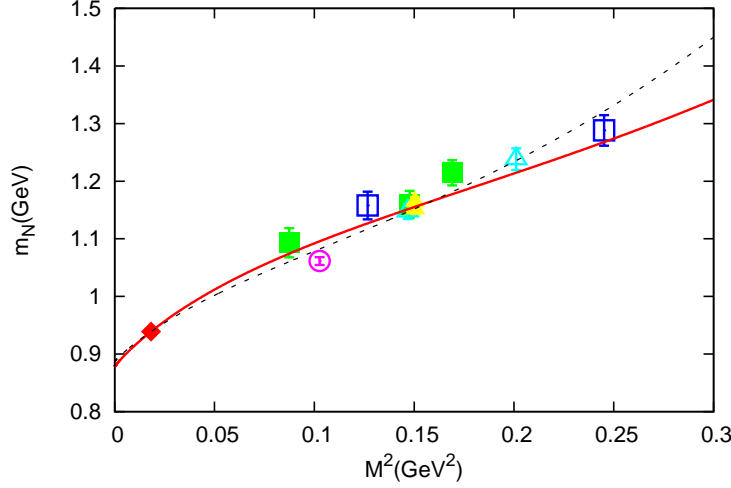


Figure 11: The nucleon mass as a function of the pion mass. The solid line denotes the result from the Fit I(c)- $O(p^4)$  and the dashed line is Fit II(c)- $O(p^4)$ . Sources of different lattice QCD data are: solid squares (PACS-CS) [45], open squares (LHPC) [46], open circles (QCDSF-UKQCD) [48], open triangles (HSC) [47], solid triangles (NPLQCD) [49]. The solid diamond is the physical point.

#### 4. Conclusions

In this paper, we performed a calculation of the pion-nucleon elastic scattering amplitude in the isospin limit within the framework of covariant baryon  $\chi$ PT using EOMS scheme up to  $O(p^4)$ . The amplitude is covariant and possesses correct analyticity and power counting properties. The resultant description of the existing partial wave phase shift data from Ref. [40] is very good for the energy in center of mass frame up to 1.13 GeV, and up to 1.20 GeV including the leading order  $\Delta(1232)$  Born-term and the partially-included  $\Delta(1232)$  loop contributions. The dimension-2, -3, and -4 LECs or their combinations are determined. The convergence properties of the chiral series are discussed. The fourth-order calculation without explicit  $\Delta(1232)$  displays a good convergence property at  $O(p^4)$  in the threshold region—the  $O(p^4)$  (NNNLO) contribution is found much smaller than the LO, NLO and NNLO ones for all the partial waves. It is certainly an improvement to the unsatisfactory situation in the third-order calculation, discussed in previous literature [23]. However, when we explicitly include the  $O(p^{3/2})$  Born term contribution of  $\Delta(1232)$  in  $\delta$ -counting [41], as well as partially the  $\Delta(1232)$  loop graphs, the convergence property is not good in the region close to the  $\Delta$  resonance, which indicates that the exact  $O(p^{7/2})$  loop contribution may be sizable and should be considered carefully in the future.

As physical applications, first, the correction to GT relation is discussed up to  $O(p^3)$ . The  $O(p^3)$  correction is much smaller (about 0.2%) than the  $O(p^2)$  correction (about 2%), which implies good convergence property of  $\Delta_{GT}$  and confirms the applicability of EOMS-B $\chi$ PT to low energy physics. Secondly, a reasonable prediction for the pion-nucleon  $\sigma$  term  $\sigma_{\pi N}$  is obtained. We find  $\sigma_{\pi N} = 52 \pm 7$  MeV from the fit without  $\Delta(1232)$ , and  $\sigma_{\pi N} = 45 \pm 6$  MeV from the fit with explicit  $\Delta(1232)$ . The two values are obtained by performing fits including the pion-nucleon partial wave phase shift data and the lattice QCD data for  $m_N$ .

## Acknowledgements

We would like to thank Li-sheng Geng for very helpful discussions and Juan Jose Sanz Cillero for a careful reading of the manuscript and valuable comments. This work is supported in part by National Nature Science Foundations of China under Contract Nos. 10925522 and 11021092. Y. H. Chen also acknowledges support by Grant Nos. 11261130311 (CRC110 by DFG and NSFC) and by NNSFC under Contract No. 11035006.

## Appendix A. $\Delta(1232)$ contribution

### Appendix A.1. Effective Lagrangian and Leading Born-term contribution

For our calculation here, the relevant effective Lagrangian with  $\Delta(1232)$  as explicit degree of freedom reads

$$\begin{aligned}\mathcal{L}_{eff}^{\Delta} &= \mathcal{L}_{RS} + \mathcal{L}_{\pi N\Delta}, \\ \mathcal{L}_{RS} &= \bar{\Delta}_{\mu} \{i\gamma^{\mu\nu\alpha} \partial_{\alpha} - m_{\Delta}\gamma^{\mu\nu}\} \Delta_{\nu}, \\ \mathcal{L}_{\pi N\Delta} &= \frac{ih_A}{2F_{\pi}m_{\Delta}} \bar{N} T_a^{\dagger} \gamma^{\mu\nu\lambda} (\partial_{\mu} \Delta_{\nu}) \partial_{\lambda} \pi^a + h.c.,\end{aligned}\quad (\text{A.1})$$

where  $T_a$  are the isospin-1/2–isospin-3/2 transition matrices satisfying  $T_a^{\dagger} T_b = \frac{2}{3}\delta_{ab} - \frac{1}{3}i\epsilon_{abc}\tau_c$ . Conventions for  $\gamma^{\mu\nu\alpha}$  and  $\gamma^{\mu\nu}$  can be consulted in Ref. [41]. The leading  $\Delta$ -exchange Born-term contribution to pion-nucleon scattering is  $O(p^{3/2})$  in the so called  $\delta$ -counting rule proposed by Ref. [41], and the Feynman diagram is shown in Fig. A.12. The

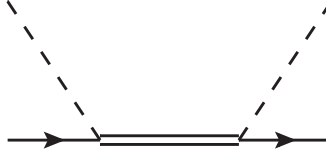


Figure A.12: Leading  $\Delta$ -exchange Born-term contribution. Double solid, solid and dashed lines represent  $\Delta$ , nucleon and pion, respectively. Crossed graph is not shown.

total contribution of leading Born-term reads

$$\begin{aligned}A_{\Delta}^{\pm}(s, t) &= A_{s\Delta}^{\pm}(s, t) \pm A_{s\Delta}^{\pm}(u, t), \\ B_{\Delta}^{\pm}(s, t) &= B_{s\Delta}^{\pm}(s, t) \mp B_{s\Delta}^{\pm}(u, t),\end{aligned}\quad (\text{A.2})$$

with

$$\begin{aligned}A_{s\Delta}^{+}(s, t) &= \frac{h_A^2}{6F_{\pi}^2 m_{\Delta}^2} \frac{s}{s - m_{\Delta}^2} \left\{ (m_N + m_{\Delta}) \left[ (M_{\pi}^2 - \frac{t}{2}) - \frac{1}{3}(s - m_N^2) \right] - \frac{s - m_N^2 + M_{\pi}^2}{3s} \left[ \frac{m_N}{2}(s - m_N^2 + M_{\pi}^2) + m_{\Delta} M_{\pi}^2 \right] \right\}, \\ B_{s\Delta}^{+}(s, t) &= \frac{h_A^2}{6F_{\pi}^2 m_{\Delta}^2} \frac{s}{s - m_{\Delta}^2} \left\{ M_{\pi}^2 - \frac{t}{2} + \frac{1}{3} [2m_N(m_N + m_{\Delta}) - M_{\pi}^2] - \frac{s - m_N^2 + M_{\pi}^2}{3s} \left[ \frac{1}{2}(s - m_N^2 + M_{\pi}^2) + m_N m_{\Delta} \right] \right\}, \\ A_{s\Delta}^{-}(s, t) &= -\frac{1}{2} A_{s\Delta}^{+}(s, t), \quad B_{s\Delta}^{-}(s, t) = -\frac{1}{2} B_{s\Delta}^{+}(s, t).\end{aligned}\quad (\text{A.3})$$

### Appendix A.2. $\Delta$ contribution to LECs and partial inclusion of the $\Delta$ loop

In order to evaluate the tree-level contribution to the LECs  $c_{1-4}$  when the  $\Delta$ -resonance is integrated out, the leading Born-term contribution is expanded in powers of  $\sigma = s - m_N^2$ ,  $M_{\pi}^2$  and  $t$ , and then compared with the  $O(p^2)$  tree amplitude Eq. B.4, leading to

$$c_1^{\Delta} = 0, \quad c_2^{\Delta} = -c_3^{\Delta} = 2c_4^{\Delta} = \frac{h_A^2 m_N^2}{9(m_{\Delta} - m_N) m_{\Delta}^2} = 1.85 \text{GeV}^{-1}, \quad (\text{A.4})$$

where we used  $h_A = 2.90$ ,  $m_N = 0.939$  GeV, and  $m_\Delta = 1.232$  GeV for the numerical value at the end of Eq. A.4. We are not able to exactly calculate pion-nucleon loop diagrams involving  $\Delta$  resonance. Nevertheless, this shortcoming can be partially remedied by substituting the  $O(p^2)$  vertices in the  $O(p^4)$  loop graphs shown in Fig. 4 by the contributions from  $\Delta$  exchanges in Eq. (A.4). The procedure is illustrated in Fig. A.13. Hence, the ‘full’ one-loop  $O(p^4)$  contribution can be given by the diagrams in Fig. 4 with a replacement<sup>9</sup>  $c_i = c'_i + c_i^\Delta$ . The effects of this replacement include only the  $O(p^{7/2})$   $\Delta$ -included loop graphs, while higher order graphs, like  $\pi N \rightarrow \pi \Delta(\text{loop}) \rightarrow \pi N$  of  $O(p^{11/2})$ , are beyond the accuracy of our calculation and therefore absent. Also, the  $O(p^{7/2})$  loop diagrams involving the  $\Delta$  propagator contributing to the self energy of nucleon can be estimated in the same way.

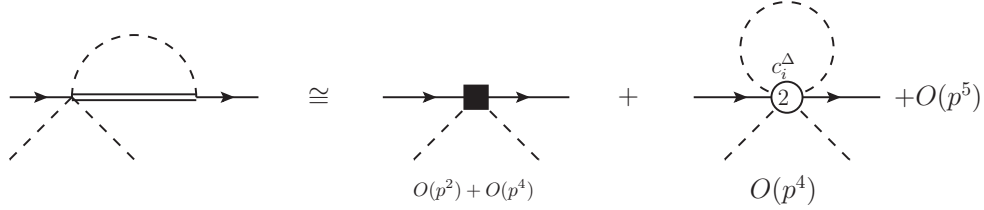


Figure A.13: Matching between  $\Delta$ -included and  $\Delta$ -less loop graphs. The circled ‘2’ vertex is related to  $c_{1-4}^\Delta$ . Possible polynomial terms (containing PCB terms), denoted by a black square, would be absorbed in the  $c_i$ ,  $d_j$ ,  $e_k$  couplings as it was done in Sec. 2.5. Barring the latter, the left-hand side  $\Delta$ -included loop graph differs from the right-hand side  $\Delta$ -less loop graph by contributions of  $O(p^5)$  and higher in the chiral expansion.

## Appendix B. Tree amplitudes

For convenience, the two independent scalar kinematical variables,  $\nu$  and  $\nu_B$ , are defined as

$$\nu = \frac{s - u}{4m_N}, \quad \nu_B = \frac{t - 2M_\pi^2}{4m_N}.$$

The Feynman graphs in Fig. 2 are calculated directly and expressed in the  $D$  and  $B$  functions, while their crossed graphs are obtained by the following crossing relations:

$$\begin{aligned} D^+(-\nu, \nu_B) &= D^+(\nu, \nu_B), & D^-(-\nu, \nu_B) &= -D^-(\nu, \nu_B); \\ B^+(-\nu, \nu_B) &= -B^+(\nu, \nu_B), & B^-(-\nu, \nu_B) &= B^-(\nu, \nu_B); \\ A^+(-\nu, \nu_B) &= A^+(\nu, \nu_B), & A^-(-\nu, \nu_B) &= -A^-(\nu, \nu_B). \end{aligned} \quad (\text{B.1})$$

Here the crossing relation for the  $A$  function is also displayed for the sake of completeness. Additionally, if the  $D$  and  $B$  functions are expressed in terms of arguments,  $s$  and  $t$ , then  $s$  should be changed to  $u$  on the right-hand side of each relation in Eq. B.1. Note that only the graphs (a), (d) and (e) in Fig. 2 have their corresponding crossed diagrams.

### Appendix B.1. $O(p)$

- Graph (a):

$$\begin{aligned} D_a^\pm &= -\frac{g^2}{4F^2} \frac{2m_N}{s - m_4^2} [\nu(\nu - \nu_B) + (m_N + m_4)\nu_B], \\ B_a^\pm &= -\frac{g^2}{4F^2} \frac{2m_N}{s - m_4^2} (\nu - \nu_B + m_N + m_4), \end{aligned} \quad (\text{B.2})$$

where  $m_4 = m - 4c_1 M^2 - 2(8e_{38} + e_{115} + e_{116})M^4$ .

<sup>9</sup>We thank J. J. Sanz Cillero for pointing it out to us.

- Graph (b):

$$\begin{aligned} D_b^+ &= 0, & D_b^- &= \frac{\nu}{2F^2}, \\ B_b^+ &= 0, & B_b^- &= \frac{1}{2F^2}. \end{aligned} \quad (\text{B.3})$$

#### Appendix B.2. $O(p^2)$

- Graph (c):

$$\begin{aligned} D_c^+ &= -\frac{4c_1 M^2}{F^2} + \frac{c_2 (16m_N^2 \nu^2 - t^2)}{8F^2 m^2} + \frac{c_3 (2M_\pi^2 - t)}{F^2}, & D_c^- &= 0, \\ B_c^+ &= 0, & B_c^- &= \frac{2c_4 m_N}{F^2}. \end{aligned} \quad (\text{B.4})$$

#### Appendix B.3. $O(p^3)$

- Graphs (d)+(e):

$$\begin{aligned} D_{de}^\pm &= -\frac{g_A M_\pi^2}{F_\pi^2} (2d_{16} - d_{18}) \left[ \nu + \frac{2m_N \nu_B}{\nu - \nu_B} \right], \\ B_{de}^\pm &= -\frac{g_A M_\pi^2}{F_\pi^2} (2d_{16} - d_{18}) \left[ 1 + \frac{2m_N}{\nu - \nu_B} \right]. \end{aligned} \quad (\text{B.5})$$

- Graph (f):

$$\begin{aligned} D_f^+ &= 0, & D_f^- &= \frac{2\nu}{F_\pi^2} \left[ 2(d_1 + d_2 + 2d_5)M_\pi^2 - (d_1 + d_2)t + 2d_3 \nu^2 \right], \\ B_f^+ &= \frac{4(d_{14} - d_{15})\nu m_N}{F_\pi^2}, & B_f^- &= 0. \end{aligned} \quad (\text{B.6})$$

#### Appendix B.4. $O(p^4)$

- Graph (g):

$$\begin{aligned} D_g^+ &= \frac{16}{F_\pi^2} \left\{ e_{14} \left( M_\pi^2 - \frac{t}{2} \right)^2 + e_{15} \left( M_\pi^2 - \frac{t}{2} \right) \nu^2 + e_{16} \nu^4 + \frac{1}{2} (2e_{19} - e_{22} - e_{36}) M_\pi^2 \left( M_\pi^2 - \frac{t}{2} \right) \right. \\ &\quad \left. + (e_{20} + e_{35}) M_\pi^2 \nu^2 + \frac{1}{2} (e_{22} - 4e_{38}) M_\pi^4 \right\}, & D_g^- &= 0, \\ B_g^+ &= 0, & B_g^- &= \frac{16m_N}{F_\pi^2} \left\{ e_{17} \left( M_\pi^2 - \frac{t}{2} \right) + e_{18} \nu^2 + \frac{1}{2} (2e_{21} - e_{37}) M_\pi^2 \right\}. \end{aligned} \quad (\text{B.7})$$

### Appendix C. One-loop Amplitudes

#### Appendix C.1. Definitions of loop functions

All the integrals appearing in the scattering amplitude up to  $O(p^4)$  level can be generalized as

$$H_{mn}^{\mu_1 \dots \mu_r} = \frac{1}{i} \int \frac{d^d k}{(2\pi)^d} \frac{k^{\mu_1} \dots k^{\mu_r}}{A_1 \dots A_m B_1 \dots B_n}, \quad (\text{C.1})$$

where  $A_i = M^2 - (k - q_i)^2 - i\epsilon$  and  $B_j = m^2 - (P_j - k)^2 - i\epsilon$  stems from the meson and nucleon propagator respectively. A standard approach to evaluate such tensor integrals has been developed by Passarino and Veltman in Ref.[34]. In this approach, the *Passarino-Veltman decomposition* is first carried out by representing the tensor integral as a sum



of independent tensor structures multiplied by scalar quantities. Then the scalar quantities are further expressed by means of initial scalar functions of the form:

$$H_{mn} = \frac{1}{i} \int \frac{d^d k}{(2\pi)^d} \frac{1}{A_1 \cdots A_m B_1 \cdots B_n} . \quad (C.2)$$

In what follows, we will specify the definitions of all the loop functions and the Passarino-Veltman decomposition formulae, with the help of the external momenta defined as

$$\begin{aligned} \Sigma_\mu &= (P + q)^\mu = (P' + q')^\mu, \\ Q^\mu &= (P' + P)^\mu, \\ \Delta_\mu &= (q' - q)^\mu = (P - P')^\mu. \end{aligned}$$

- 1 meson:  $\Delta_\pi = H_{10}$

$$\begin{aligned} \Delta_\pi, \Delta_\pi^\mu, \Delta_\pi^{\mu\nu} &= \frac{1}{i} \int \frac{d^d k}{(2\pi)^d} \frac{\{1, k^\mu, k^{\mu\nu}\}}{M^2 - k^2}, \\ \Delta_\pi^\mu &= 0, \\ \Delta_\pi^{\mu\nu} &= g^{\mu\nu} \Delta_\pi^{(2)}, \end{aligned}$$

where

$$\begin{aligned} \Delta_\pi &= \frac{M^2}{16\pi^2} \left\{ R + \ln \frac{M^2}{\mu^2} \right\}, R = \frac{2}{d-4} + \gamma_E - 1 - \ln 4\pi, \\ \Delta_\pi^{(2)} &= \frac{M^2}{d} \Delta_\pi = \frac{M^2}{4} \left( \Delta_\pi - \frac{M^2}{32\pi^2} \right). \end{aligned} \quad (C.3)$$

- 1 nucleon:  $\Delta_N = H_{01}$

$$\begin{aligned} \{\Delta_N, \Delta_N^\mu, \Delta_N^{\mu\nu}\} &= \frac{1}{i} \int \frac{d^d k}{(2\pi)^d} \frac{\{1, k^\mu, k^\mu k^\nu\}}{m^2 - (\Sigma - k)^2}, \\ \Delta_N^\mu &= \Sigma^\mu \Delta_N, \\ \Delta_N^{\mu\nu} &= g^{\mu\nu} \Delta_N^{(2)} + \Sigma^\mu \Sigma^\nu \Delta_N, \end{aligned}$$

where

$$\begin{aligned} \Delta_N &= \frac{m^2}{16\pi^2} \left\{ R + \ln \frac{m^2}{\mu^2} \right\}, R = \frac{2}{d-4} + \gamma_E - 1 - \ln 4\pi, \\ \Delta_N^{(2)} &= \frac{m^2}{d} \Delta_N = \frac{m^2}{4} \left( \Delta_N - \frac{m^2}{32\pi^2} \right). \end{aligned} \quad (C.4)$$

- 2 mesons:  $J = H_{20}$

$$\begin{aligned} \{J, J^\mu, J^{\mu\nu}\} &= \frac{1}{i} \int \frac{d^d k}{(2\pi)^d} \frac{\{1, k^\mu, k^\mu k^\nu\}}{[M^2 - k^2] [M^2 - (k - \Delta)^2]}, \\ J^\mu(t) &= \frac{1}{2} \Delta^\mu J(t), \\ J^{\mu\nu}(t) &= (\Delta^\mu \Delta^\nu - g^{\mu\nu} \Delta^2) J^{(1)}(t) + \Delta^\mu \Delta^\nu J^{(2)}(t), \end{aligned}$$

where

$$\begin{aligned} J^{(1)}(t) &= \frac{1}{(1-d)t} \left\{ -\frac{1}{2} \Delta_\pi + \left( M^2 - \frac{1}{4} t \right) J(t) \right\} \\ &= -\frac{1}{3t} \left\{ -\frac{1}{2} \Delta_\pi + \left( M^2 - \frac{1}{4} t \right) J(t) + \frac{1}{16\pi^2} \left( M^2 - \frac{1}{6} t \right) \right\}, \\ J^{(2)}(t) &= \frac{1}{2t} \left\{ -\Delta_\pi + \frac{1}{2} t J(t) \right\}. \end{aligned}$$

- 1 meson, 1 nucleon:  $H = H_{11}$

$$\begin{aligned}\{H, H^\mu, H^{\mu\nu}, \tilde{H}^\mu, H^{\mu\nu\rho}\} &= \frac{1}{i} \int \frac{d^d k}{(2\pi)^d} \frac{\{1, k^\nu, k^\mu k^\nu, k^\mu k^2, k^\mu k^\nu k^\rho\}}{[M^2 - k^2] [m^2 - (\Sigma - k)^2]}, \\ H^\mu(s) &= \Sigma^\mu H^{(1)}(s), \\ H^{\mu\nu}(s) &= g^{\mu\nu} H^{(2)}(s) + \Sigma^\mu \Sigma^\nu H^{(3)}(s), \\ \tilde{H}^\mu(s) &= \Sigma^\mu \tilde{H}^{(1)}(s), \\ H^{\mu\nu\rho}(s) &= (g^{\mu\nu} \Sigma^\rho + g^{\nu\rho} \Sigma^\mu + g^{\rho\mu} \Sigma^\nu) H^{(4)}(s) + \Sigma^\mu \Sigma^\nu \Sigma^\rho H^{(5)}(s),\end{aligned}$$

where

$$\begin{aligned}H^{(1)}(s) &= \frac{1}{2s} \left\{ \Delta_\pi - \Delta_N + (s - m^2 + M^2) H(s) \right\}, \\ H^{(2)}(s) &= \frac{1}{d-1} \left\{ -\frac{1}{2} \Delta_N + M^2 H(s) - \frac{1}{2} (s - m^2 + M^2) H^{(1)}(s) \right\}, \\ &= \frac{1}{3} \left\{ -\frac{1}{2} \Delta_N + M^2 H(s) - \frac{1}{2} (s - m^2 + M^2) H^{(1)}(s) + \frac{M^2 + m^2 - \frac{1}{3}s}{32\pi^2} \right\}, \\ H^{(3)}(s) &= \frac{1}{s} \left\{ -\Delta_N + M^2 H(s) - d H^{(2)}(s) \right\}, \\ &= \frac{1}{3s} \left\{ -\Delta_N - M^2 H(s) + 2(M^2 + s - m^2) H^{(1)}(s) - \frac{M^2 + m^2 - \frac{1}{3}s}{32\pi^2} \right\}, \\ \tilde{H}^{(1)}(s) &= -\Delta_N + M^2 H^{(1)}(s), \\ H^{(4)}(s) &= \frac{1}{2s} \left\{ \Delta_\pi^{(2)} - \Delta_N^{(2)} + (s - m^2 + M^2) H^{(2)}(s) \right\}, \\ H^{(5)}(s) &= \frac{1}{2s} \left\{ -\Delta_N + (s - m^2 + M^2) H^{(3)}(s) - 4 H^{(4)}(s) \right\}.\end{aligned}$$

- 2 nucleons:  $J_N = H_{02}$

$$\begin{aligned}\{J_N, J_N^\mu, J_N^{\mu\nu}\} &= \frac{1}{i} \int \frac{d^d k}{(2\pi)^d} \frac{\{1, k^\mu, k^\mu k^\nu\}}{[m^2 - (k - P)^2] [m^2 - (k - P')^2]}, \\ J_N^\mu(t) &= \frac{1}{2} Q^\mu J_N(t), \\ J_N^{\mu\nu}(t) &= (\Delta^\mu \Delta^\nu - g^{\mu\nu} \Delta^2) J_N^{(1)}(t) + \Delta^\mu \Delta^\nu J_N^{(2)}(t) + \frac{1}{2} (P^\mu P'^\nu + P^\nu P'^\mu) J_N(t),\end{aligned}$$

where

$$\begin{aligned}J_N^{(1)}(t) &= \frac{1}{(1-d)t} \left\{ -\frac{1}{2} \Delta_N + \left( m^2 - \frac{1}{4} t \right) J_N(t) \right\} \\ &= -\frac{1}{3t} \left\{ -\frac{1}{2} \Delta_N + \left( m^2 - \frac{1}{4} t \right) J_N(t) + \frac{1}{16\pi^2} \left( m^2 - \frac{1}{6} t \right) \right\}, \\ J_N^{(2)}(t) &= \frac{1}{2t} \left\{ -\Delta_N + \frac{1}{2} t J_N(t) \right\}.\end{aligned}$$

- 3 nucleons:

$$H_{03} = \frac{1}{i} \int \frac{d^d k}{(2\pi)^d} \frac{1}{[m^2 - (P - k)^2] [m^2 - (k - \Sigma)^2] [m - (P' - k)^2]}.$$

- 2 mesons, 1 nucleon:

$$\begin{aligned}\{H_{21}, H_{21}^\mu, H_{21}^{\mu\nu}\} &= \frac{1}{i} \int \frac{d^d k}{(2\pi)^d} \frac{\{1, k^\nu, k^\mu k^\nu\}}{[M^2 - k^2] [M^2 - (k - \Delta)^2] [m - (P - k)^2]}, \\ H_{21}^\mu(t) &= Q^\mu H_{21}^{(1)}(t) + \frac{1}{2} \Delta^\mu H_{21}(t), \\ H_{21}^{\mu\nu}(t) &= g^{\mu\nu} H_{21}^{(2)}(t) + Q^\mu Q^\nu H_{21}^{(3)}(t) + \Delta^\mu \Delta^\nu H_{21}^{(4)}(t) + (\Delta^\mu Q^\nu + Q^\mu \Delta^\nu) \frac{1}{2} H_{21}^{(1)}(t),\end{aligned}$$

where

$$\begin{aligned}H_{21}^{(1)}(t) &= \frac{1}{4m^2 - t} \left\{ J(t) - H(m^2) + \left( M^2 - \frac{1}{2}t \right) H_{21}(t) \right\}, \\ H_{21}^{(2)}(t) &= \frac{1}{(d-2)} \left\{ \frac{1}{2} M^2 H_{21}(t) - (M^2 - 2m^2) H_{21}^{(1)}(t) - \frac{1}{2} J(t) \right\}, \\ &= \frac{1}{2} \left\{ \frac{1}{2} M^2 H_{21}(t) - (M^2 - 2m^2) H_{21}^{(1)}(t) - \frac{1}{2} J(t) \right\} - \frac{1}{64\pi^2}, \\ H_{21}^{(3)}(t) &= \frac{1}{4m^2 - t} \left\{ -\frac{1}{2} H^{(1)}(m^2) + \left( M^2 - \frac{1}{2}t \right) H_{21}^{(1)}(t) - H_{21}^{(2)}(t) \right\}, \\ H_{21}^{(4)}(t) &= \frac{1}{t} \left\{ \frac{1}{2} H^{(1)}(m^2) - \frac{1}{2} H(m^2) + \frac{1}{4} t H_{21}(t) - H_{21}^{(2)}(t) \right\}.\end{aligned}$$

- 1 mesons, 2 nucleon:  $H_A$

$$\begin{aligned}\{H_A, H_A^\mu, H_A^{\mu\nu}\} &= \frac{1}{i} \int \frac{d^d k}{(2\pi)^d} \frac{\{1, k^\nu, k^\mu k^\nu\}}{[M^2 - k^2] [m^2 - (P - k)^2] [m - (P' - k)^2]}, \\ H_A^\mu(t) &= Q^\mu H_A^{(1)}(t), \\ H_A^{\mu\nu}(t) &= g^{\mu\nu} H_A^{(2)}(t) + Q^\mu Q^\nu H_A^{(3)}(t) + \Delta^\mu \Delta^\nu H_A^{(4)}(t),\end{aligned}$$

where

$$\begin{aligned}H_A^{(1)}(t) &= \frac{1}{4m^2 - t} \left\{ H(m^2) - J_N(t) + M^2 H_A \right\}, \\ H_A^{(2)}(t) &= \frac{1}{d-2} \left\{ M^2 H_A(t) - M^2 H_A^{(1)}(t) - \frac{1}{2} J_N(t) \right\}, \\ &= \frac{1}{2} \left\{ M^2 H_A(t) - M^2 H_A^{(1)}(t) - \frac{1}{2} J_N(t) - \frac{1}{32\pi^2} \right\}, \\ H_A^{(3)}(t) &= \frac{1}{4m^2 - t} \left\{ \frac{1}{2} H^{(1)}(m^2) - \frac{1}{2} J_N(t) + M^2 H_A^{(1)}(t) - H_A^{(2)}(t) \right\}, \\ H_A^{(4)}(t) &= -\frac{1}{t} \left\{ \frac{1}{2} H^{(1)}(m^2) + H_A^{(2)}(t) \right\}.\end{aligned}$$

- 1 mesons, 2 nucleon:  $H_B$

$$\begin{aligned}\{H_B, H_B^\mu, H_B^{\mu\nu}\} &= \frac{1}{i} \int \frac{d^d k}{(2\pi)^d} \frac{\{1, k^\mu, k^\mu k^\nu\}}{[M^2 - k^2] [m^2 - (P - k)^2] [m - (\Sigma - k)^2]}, \\ H_B^\mu(s) &= (P + \Sigma)^\mu H_B^{(1)}(s) + (P - \Sigma)^\mu H_B^{(2)}(s), \\ H_B^{\mu\nu}(s) &= g^{\mu\nu} H_B^{(3)}(s) + (P + \Sigma)^\mu (P + \Sigma)^\nu H_B^{(4)}(s) + (P - \Sigma)^\mu (P - \Sigma)^\nu H_B^{(5)}(s) + 2(P^\mu P^\nu - \Sigma^\mu \Sigma^\nu) H_B^{(6)}(s),\end{aligned}$$

where

$$H_B^{(1)}(s) = -\frac{1}{2\lambda(s, m^2, M^2)} \left\{ [M^2 - (m^2 - s)] H(s) + [M^2 + (m^2 - s)] H(m^2) - 2M^2 J_N(M^2) \right. \\ \left. + [(s - m^2 + 2M^2)M^2 - (m^2 - s)^2] H_B(s) \right\}, \quad (C.5)$$

$$H_B^{(2)}(s) = -\frac{1}{2\lambda(s, m^2, M^2)} \left\{ [m^2 - M^2 + 3s] H(s) + [M^2 - 3m^2 - s] H(m^2) + 2(m^2 - s) J_N(M^2) \right. \\ \left. + (m^2 - s)(3m^2 - 3M^2 + s) H_B(s) \right\}, \quad (C.6)$$

$$H_B^{(3)}(s) = -\frac{1}{2-d} \frac{1}{2\lambda(s, m^2, M^2)} \left\{ M^2 (3m^2 - 3M^2 + s) J_N(M^2) + [(s - m^2)(2m^2 - M^2) + M^4] H(m^2) \right. \\ \left. + [m^4 - s^2 + M^4 + 2M^2(s - m^2)] H(s) + 2[m^6 + 2M^6 - 2m^4s - M^4s + m^2(s^2 - 3M^4)] H_B(s) \right\},$$

$$H_B^{(4)}(s) = \frac{1}{4\lambda(s, m^2, M^2)} \left\{ (s - m^2)(H(m^2) - H(s)) + (s - m^2 - M^2)H^{(1)}(m^2) - (s - m^2 + M^2)H^{(1)}(s) \right. \\ \left. + 4M^2 J_N(M^2) + ((s - m^2)^2 - 4M^4) H_B(s) - 4(1 - d)M^2 H_B^{(3)}(s) \right\},$$

$$H_B^{(5)}(s) = \frac{1}{4\lambda(s, m^2, M^2)} \left\{ 2(s + 3m^2 - 3M^2) J_N(M^2) + (s - m^2 + 2M^2)(H(m^2) + H(s)) + (s + 3m^2 - M^2)H^{(1)}(m^2) \right. \\ \left. + (3s + m^2 - M^2)H^{(1)}(s) + ((s - m^2)^2 - 4M^2(s + 3m^2 - 2M^2)) I_B(s) - 4(1 - d)(2s + 2m^2 - M^2)H_B^{(3)}(s) \right\}$$

$$H_B^{(6)}(s) = \frac{1}{4\lambda(s, m^2, M^2)} \left\{ (s - m^2)(2J_N(M^2) + H(m^2) + H(s)) + (s + 3m^2 - M^2)H^{(1)}(m^2) \right. \\ \left. - (3s + m^2 - M^2)H^{(1)}(s) + (s - m^2)(s - m^2 - 2M^2)H_B(s) - 4(1 - d)(s - m^2)H_B^{(3)}(s) \right\}.$$

- 1 mesons, 3 nucleon:

$$\{H_{13}, H_{13}^\mu\} = \frac{1}{i} \int \frac{d^d k}{(2\pi)^d} \frac{\{1, k^\mu\}}{[M^2 - k^2][m^2 - (P - k)^2][m - (\Sigma - k)^2][m^2 - (P' - k)^2]}, \\ H_{13}^\mu(s, t) = \mathcal{Q}^\mu H_{13}^{(1)}(s, t) + (\Delta + 2q)^\mu H_{13}^{(2)}(s, t),$$

where

$$H_{13}^{(1)}(s, t) = -\frac{1}{\lambda(s, m^2, M^2) + st} \left\{ (s - m^2 + M^2)H_B(s) - \frac{1}{2}(s - u)H_A(t) \right. \\ \left. - \left[ \frac{1}{2}(s + u) - (m^2 - M^2) \right] H_{03}(t) + (s - m^2 + M^2) \left[ M^2 - \frac{1}{2}(s - u) \right] H_{13}(s, t) \right\}, \\ H_{13}^{(2)}(s, t) = \frac{1}{s - u} \left\{ H_B(s) - H_{03}(t) + M^2 H_{13}(s, t) - (4m^2 - t)H_{13}^{(1)}(s, t) \right\}.$$

After removing parts proportional to  $R = \frac{2}{d-4} + \gamma_E - 1 - \ln 4\pi$ , the remaining scalar integrals are finite and denoted by, e.g.  $\bar{H}(s)$ ,  $\bar{J}_N(t)$ ,  $\bar{H}_A(t)$ , etc..

### Appendix C.2. $O(p^3)$ results

The contributions from the  $O(p^3)$  loop graphs shown in Fig. 3 are displayed below, respectively. The total  $O(p^3)$  loop contributions are given by

$$A_{total}^\pm = \sum_G [A_G^\pm(s, t) \pm A_G^\pm(u, t)] + \sum_H A_H^\pm(s, t), \quad G \in \{a, \dots, i, n, \dots, s\}, \\ B_{total}^\pm = \sum_G [B_G^\pm(s, t) \mp B_G^\pm(u, t)] + \sum_H B_H^\pm(s, t), \quad H \in \{k, l, m, t, u, v\}, \quad (C.7)$$

where the  $A_G^\pm(u, t)$  and  $B_G^\pm(u, t)$  ( $G \in \{a, \dots, i, \dots, s\}$ ) are obtained from the graphs  $(a), \dots, (i), (n) \dots, (s)$  through crossing.

The abbreviation  $F(s)$  in the amplitudes is defined as

$$F(s) \equiv 2(\Delta_N - M^2 H(s)) + (s - m^2) H^{(1)}(s) .$$

- Graphs (a)+(b):

$$\begin{aligned} A_{ab}^\pm &= \frac{mg^2}{2F^4} F(s) , \\ B_{ab}^\pm &= -\frac{g^2}{2F^4} \left\{ \frac{2m^2 F(s)}{s - m^2} - (\Delta_N - M^2 H(s)) + F(s) \right\} . \end{aligned}$$

- Graphs (c)+(d):

$$\begin{aligned} A_{cd}^\pm &= \frac{mg^4}{8F^4} \left\{ -2\Delta_\pi + (s - m^2) H^{(1)}(s) - 8m^2 \left[ - (J_N(M^2) - M^2 H_B(s)) + (s - m^2) H_B^{(2)}(s) \right] \right\} , \\ B_{cd}^\pm &= \frac{g^4}{8F^4} \left\{ (\Delta_N - M^2 H(s)) + (s - m^2) (H^{(1)}(s) - 4m^2 H_B^{(1)}(s)) \right. \\ &\quad \left. + \frac{4m^2}{s - m^2} \left[ \Delta_\pi + (s + 3m^2) (- (J_N(M^2) - M^2 H_B(s)) + (s - m^2) H_B^{(2)}(s)) \right] \right\} . \end{aligned}$$

- Graph (e):

$$\begin{aligned} A_e^\pm &= \frac{3g^4 m}{16F^4} \left\{ \frac{4m^2 F(s)}{m^2 - s} - 3F(s) + 2(\Delta_N - M^2 H(s)) \right\} , \\ B_e^\pm &= \frac{3g^4}{16F^4} \left\{ F(s) - (\Delta_N - M^2 H(s)) - \frac{4m^2}{m^2 - s} \left[ 2F(s) - (\Delta_N - M^2 H(s)) \right] + \frac{8m^4}{(s - m^2)^2} F(s) \right\} . \end{aligned}$$

- Graph (f):

$$\begin{aligned} A_f^+ &= \frac{1}{2F^4} m (s - m^2) H^{(1)}(s) , \\ B_f^+ &= \frac{1}{8F^4} \left\{ 4(s - m^2) H^{(1)}(s) + 4(\Delta_N - M^2 H(s)) - \Delta_\pi \right\} , \\ A_f^- &= \frac{1}{2} A_{3f}^+ , \quad B_f^- = \frac{1}{2} B_{3f}^+ . \end{aligned}$$

- Graphs (g)+(h):

$$\begin{aligned} A_{gh}^+ &= \frac{mg^2}{2F^4} (s - m^2) \left\{ -2H(s) + H^{(1)}(s) + 8m^2 H_B^{(1)}(s) \right\} , \\ B_{gh}^+ &= \frac{g^4}{4F^4} \left\{ (\Delta_N - M^2 H(m^2)) - 2\Delta_\pi + 8m^2 \left[ J_N(M^2) - M^2 H_B(s) \right] \right. \\ &\quad \left. + 2(m^2 - s) \left[ H(s) - H^{(1)}(s) - 4m^2 (H_B^{(1)}(s) - H_B^{(2)}(s)) \right] \right\} , \\ A_{gh}^- &= 0 , \quad B_{gh}^- = 0 . \end{aligned}$$

- Graph (i):

$$\begin{aligned}
A_i^+ &= \frac{3mg^4}{16F^4} \left\{ 2M^2 [H(m^2) - H(s)] + (s - m^2) [2H(s) + H^{(1)}(s)] \right. \\
&\quad + 8m^2 [J_N(t) - M^2 H_A(t)] + 4m^2 H_A^{(1)}(t) - (s - u) H_A^{(3)}(t) \\
&\quad - (J_N(M^2) - M^2 H_B(s)) - M^2 (H_B^{(1)}(s) - H_B^{(2)}(s)) - (m^2 + 3s) H_B^{(1)}(s) + (s - m^2) H_B^{(2)}(s) \\
&\quad \left. + 32m^4 (s - m^2) H_{13}^{(1)}(s, t) \right\} , \\
B_i^+ &= \frac{3g^4}{16F^4} \left\{ (3m^2 + s) H(s) + 4m^2 H^{(1)}(m^2) - (m^2 + s) H^{(1)}(s) \right. \\
&\quad + 4m^2 [- (J_N(t) - M^2 H_A(t)) - 2H_A^{(2)}(t) - 2 (J_N(M^2) - M^2 H_B(s)) - 2 (3m^2 + s) H_B^{(1)}(s) \\
&\quad \left. - 2 (m^2 - s) H_B^{(2)}(s)] + 16m^4 [H_{03}(t) - M^2 H_{13}(s, t) + 2 (s - m^2) H_{13}^{(2)}(s, t)] \right\} , \\
A_i^- &= -\frac{1}{3} A_i^+ , \quad B_i^- = -\frac{1}{3} B_i^+ .
\end{aligned}$$

- Graph (k):

$$A_k^\pm = B_k^+ = 0 , \quad B_k^- = \frac{t}{F^4} J^{(1)}(t) .$$

- Graph (l):

$$\begin{aligned}
A_l^+ &= \frac{mg^2}{6F^4} \left\{ 4 [\Delta_N - M^2 H(m^2)] - 3 (M^2 - 2t) [J(t) - 4m^2 H_{21}^{(1)}(t)] \right\} , \\
B_l^+ &= 0 , \\
A_l^- &= -\frac{4m^3 g^2}{F^4} (s - u) H_{21}^{(3)}(t) , \\
B_l^- &= -\frac{g^2}{F^4} \left\{ t J^{(1)}(t) + 4m^2 H_{21}^{(2)}(t) \right\} .
\end{aligned}$$

- Graph (m):

$$\begin{aligned}
A_m^+ &= B_m^+ = 0 , \\
A_m^- &= -\frac{g^2 m^3}{F^4} (s - u) H_A^{(3)}(t) , \\
B_m^- &= -\frac{g^2}{8F^4} \left\{ \Delta_\pi - 4m^2 [H^{(1)}(m^2) - (J_N(t) - M^2 H_A(t)) - 2H_A^{(2)}(t)] \right\} .
\end{aligned}$$

- Graphs (n)+(o):

$$\begin{aligned}
A_{no}^\pm &= \frac{mg^2}{F^4} \left\{ \Delta_N - M^2 H(m^2) \right\} , \\
B_{no}^\pm &= A_{no}^\pm \left\{ \frac{2m}{m^2 - s} - \frac{1}{4m} \right\} .
\end{aligned}$$

- Graphs (p)+(r):

$$\begin{aligned}
A_{pr}^\pm &= -\frac{mg^2}{3F^4} \Delta_\pi , \\
B_{pr}^\pm &= A_{pr}^\pm \left\{ \frac{2m}{m^2 - s} - \frac{1}{2m} \right\} .
\end{aligned}$$

- Graph (s):

$$A_s^\pm = B_s^\pm = 0 .$$

- Graphs (t)+(u):

$$\begin{aligned} A_{tu}^+ &= -\frac{2mg^2}{3F^4} \{ \Delta_N - M^2 H(m^2) \} , \\ B_{tu}^- &= -\frac{3}{4m} A_{tu}^+ , \\ A_{tu}^- &= 0 , \quad B_{tu}^+ = 0 . \end{aligned}$$

- Graph (v):

$$\begin{aligned} A_v^\pm &= B_v^\pm = 0 , \\ B_v^- &= -\frac{5}{24F^4} \Delta_\pi . \end{aligned}$$

### Appendix C.3. $O(p^4)$ results

The contributions from the  $O(p^4)$  loop graphs shown in Fig. 4 are displayed below. The total  $O(p^4)$  loop contributions are given by

$$\begin{aligned} A_{total}^\pm &= \sum_G [A_G^\pm(s, t) \pm A_G^\pm(u, t)] + \sum_H A_H^\pm(s, t) , \quad G \in \{a, b, f1, f2, g, h, n, o, s\} , \\ B_{total}^\pm &= \sum_G [B_G^\pm(s, t) \mp B_G^\pm(u, t)] + \sum_H B_H^\pm(s, t) , \quad H \in \{k, m, v\} , \end{aligned} \quad (C.8)$$

where the  $A_G^\pm(u, t)$  and  $B_G^\pm(u, t)$  ( $G \in \{a, b, f1, f2, g, h, n, o, s\}$ ) are obtained from the graphs (a), (b), (f1), (f2), (g), (h), (n), (o), (s) through crossing.

- Graphs (a)+(b):

$$\begin{aligned}
A_{ab}^{\pm} &= \frac{2c_1 g^2 M^2}{F^4} \left\{ (s - m^2) H^{(1)}(s) + \Delta_N - M^2 H(s) \right\} \\
&\quad - \frac{c_2 g^2}{8F^4 m^2} \left\{ 2(s + 3m^2) \Delta_N^{(2)} - M^2 (s - m^2 + M^2) \Delta_\pi - 2(M^2 - 4m^2) \Delta_\pi^{(2)} \right. \\
&\quad \left. + 2(s - m^2 - M^2) \left[ \frac{1}{2} (s - m^2 + M^2) (\Delta_N - M^2 H(s) + (s - m^2) H^{(1)}(s)) \right. \right. \\
&\quad \left. \left. - (m^2 - M^2) \tilde{H}^{(1)}(s) + (s + 7m^2 - 2M^2) H^{(2)}(s) + (m^2 - M^2) (s - m^2) H^{(3)}(s) \right] \right\} \\
&\quad - \frac{(c_3 + c_4) g^2}{F^4} \left\{ -\frac{1}{2} (s - m^2 + M^2) \tilde{H}^{(1)}(s) + (M^2 - 4m^2) H^{(2)}(s) + \frac{1}{2} (s - m^2) (s - m^2 + M^2) H^{(3)}(s) \right\} \\
&\quad + \frac{c_4 g^2}{F^4} \left\{ (s - m^2) (s + m^2) H^{(1)}(s) + (s + 3m^2) (\Delta_N - M^2 H(s)) \right\} \\
B_{ab}^{\pm} &= -\frac{2c_1 g^2 m M^2}{F^4 (s - m^2)} \left\{ 2 (\Delta_N - M^2 H(s)) + (s - m^2) H^{(1)}(s) \right\} \\
&\quad - \frac{c_2 g^2}{2F^4 m (s - m^2)} \left\{ -2(s + m^2) \Delta_N^{(2)} + \frac{1}{2} M^2 (s - m^2 + M^2) \Delta_\pi - (s + 3m^2 - M^2) \Delta_\pi^{(2)} \right. \\
&\quad \left. + \frac{1}{2} (m^2 - s + M^2) \left[ \frac{1}{2} (s - m^2 + M^2) (2(\Delta_N - M^2 H(s)) + (s - m^2) H^{(1)}(s)) \right. \right. \\
&\quad \left. \left. - 2(m^2 - M^2) \tilde{H}^{(1)}(s) + (5s + 11m^2 - 4M^2) H^{(2)}(s) + (m^2 - M^2) (s - m^2) H^{(3)}(s) \right] \right\} \\
&\quad - \frac{(c_3 + c_4) g^2 m}{F^4 (s - m^2)} \left\{ (s - m^2 + M^2) \tilde{H}^{(1)}(s) + 2(s + 3m^2 - M^2) H^{(2)}(s) - \frac{1}{2} (s - m^2) (s - m^2 + M^2) H^{(3)}(s) \right\} \\
&\quad - \frac{c_4 g^2 m}{F^4 (s - m^2)} \left\{ 4(s + m^2) (\Delta_N - M^2 H(s)) + (s - m^2) (3s + m^2) H^{(1)}(s) \right\} \tag{C.9}
\end{aligned}$$

- Graphs (f1)+(f2):

$$\begin{aligned}
A_f^+ &= \frac{c_4}{F^4} \left\{ (m^2 - s) [\Delta_N + \Delta_\pi + (s - m^2 - M^2) H(s)] + 2m^2 (s - m^2) H^{(1)}(s) + (m^2 - s + M^2) H^{(2)}(s) \right. \\
&\quad \left. + \frac{1}{2} (s - m^2 + M^2) [\Delta_N + (s - m^2 - M^2) H^{(1)}(s)] + m^2 (s - m^2 + M^2) H^{(3)}(s) \right\} \\
A_f^- &= \frac{1}{2} A_f^+ - \frac{2c_1 M^2}{F^4} \left\{ \Delta_N + (s - m^2 - M^2) H(s) + 2m^2 H^{(1)}(s) \right\} \\
&\quad + \frac{c_2}{2F^4 m^2} \left\{ (s - m^2) \Delta_N^{(2)} + \frac{1}{2} (s - m^2 - M^2) \left[ \frac{1}{2} (s - m^2 + M^2) \Delta_\pi + \Delta_\pi^{(2)} \right] \right. \\
&\quad + \frac{1}{4} (s - m^2 - M^2) (s - m^2 + M^2) [\Delta_N + (s - m^2 - M^2) H(s) + 2m^2 H^{(1)}(s)] \\
&\quad + \frac{1}{2} (s - m^2 - M^2) [(m^2 - M^2) (\Delta_N + (s - m^2 - M^2) H^{(1)}(s)) + 2(s - M^2) H^{(2)}(s) + 2m^2 (m^2 - M^2) H^{(3)}(s)] \\
&\quad \left. + \frac{c_3}{F^4} \left\{ \frac{1}{2} (s - m^2 + M^2) [\Delta_N + (s - m^2 - M^2) H^{(1)}(s)] - (s - m^2 - M^2) H^{(2)}(s) + m^2 (s - m^2 + M^2) H^{(3)}(s) \right\} \right\} \\
B_f^+ &= \frac{c_4}{F^4} \left\{ 2m [\Delta_N + \Delta_\pi + (s - m^2 - M^2) H(s)] - 2m (s + m^2) H^{(1)}(s) + 4m H^{(2)}(s) + m (s - m^2 + M^2) H^{(3)}(s) \right\} \\
B_f^- &= \frac{1}{2} B_f^+ - \frac{4c_1 m M^2}{F^4} H^{(1)}(s) + \frac{c_2}{2F^4 m^2} \left\{ -2m (\Delta_N^{(2)} + \Delta_\pi^{(2)}) + \frac{1}{2} m (s - m^2 - M^2) (s - m^2 + M^2) H^{(1)}(s) \right. \\
&\quad \left. + \frac{1}{2} (s - m^2 - M^2) [-6m H^{(2)}(s) + 2m (m^2 - M^2) H^{(3)}(s)] \right\} + \frac{2c_3 m}{F^4} \left\{ 2H^{(2)}(s) + \frac{1}{2} (s - m^2 + M^2) H^{(3)}(s) \right\}
\end{aligned}$$



- Graphs (g)+(h):

$$\begin{aligned}
A_{gh}^+ &= -\frac{2c_1g^2M^2}{F^4} \left\{ (s-m^2)H(s) + 2m^2H^{(1)}(m^2) - (s+m^2)H^{(1)}(s) + 4m^2M^2(H_B^{(2)}(s) - H_B^{(1)}(s)) \right\} \\
&+ \frac{c_2g^2}{2F^4} \left\{ \frac{s-m^2}{2m^2}(\Delta_N^{(2)} + \Delta_\pi^{(2)}) + \frac{s-m^2}{4m^2}(s-m^2+M^2)\Delta_\pi + (2M^2-t)\Delta_N \right. \\
&\quad - \frac{1}{2}M^2(2M^2-t)J_N(M^2) + M^2(2(s-m^2-M^2)+t)J_N^{(1)}(M^2) + M^2(2M^2-t)J_N^{(2)}(M^2) \\
&\quad + 2(2M^2-t)H^{(2)}(m^2) + \left[ M^2(m^2+M^2-u) + \frac{1}{2}(s-m^2-M^2)(2m^2-t) \right] H^{(3)}(m^2) \\
&\quad + \frac{1}{2}(s-m^2+M^2) \left[ -2M^2H^{(1)}(m^2) + (s+m^2-M^2)H^{(3)}(m^2) \right] - (2M^2+s-u)H^{(4)}(m^2) \\
&\quad - \frac{1}{2}(m^2-M^2+s)(m^2+M^2-u)H^{(5)}(m^2) + \frac{(s-m^2-M^2)}{4m^2} \left[ (s-m^2)(s-m^2+M^2)H(s) \right. \\
&\quad + 2(s-3m^2)H^{(2)}(s) - \left. \left( (s-m^2)^2 + M^2(3s-m^2) \right) H^{(1)}(s) - 2(m^2-M^2)(s+m^2)H^{(3)}(s) \right] \\
&\quad - (s-m^2-M^2) \left[ M^2(s-m^2+M^2)(H_B^{(1)}(s) - H_B^{(2)}(s)) - 2(2u-2m^2-M^2)H_B^{(3)}(s) \right. \\
&\quad \left. - M^2(s-5m^2+M^2+2t)(H_B^{(4)}(s) - H_B^{(6)}(s)) + M^2(s-m^2-3M^2+2t)(H_B^{(5)}(s) - H_B^{(6)}(s)) \right] \Big\} \\
&+ \frac{(c_3-c_4)g^2}{F^4} \left\{ (s-m^2) \left( \frac{1}{2}(s-m^2+M^2)H^{(1)}(s) - H^{(2)}(s) \right) + m^2(m^2+M^2-u)H^{(3)}(m^2) \right. \\
&\quad - \frac{1}{2}(s+m^2)(s-m^2+M^2)H^{(3)}(s) - 2m^2 \left[ 2(m^2-s+2M^2-t)H_B^{(3)}(s) \right. \\
&\quad \left. + M^2(2M^2+s-u)(H_B^{(4)}(s) - H_B^{(6)}(s)) - M^2(2m^2-s-u)(H_B^{(5)}(s) - H_B^{(6)}(s)) \right] \Big\} \\
&+ \frac{c_4g^2}{F^4}(s-m^2) \left\{ \Delta_\pi - (s-m^2)(H^{(1)}(s) - H(s)) - 4m^2 \left( J_N(M^2) - M^2H_B(s) \right) - 4m^2(s-m^2)(H_B^{(1)}(s) - H_B^{(2)}(s)) \right\}, \\
A_{gh}^- &= -A_{gh}^+ \quad (c_4 = 0). \\
B_{gh}^+ &= -\frac{4c_1g^2mM^2}{F^4} \left\{ J_N(M^2) - M^2H_B(s) - \frac{1}{2}H^{(1)}(s) + (s-m^2-M^2)(H_B^{(1)}(s) - H_B^{(2)}(s)) \right\} \\
&+ \frac{c_2g^2}{2F^4m} \left\{ -(t-2M^2)\Delta_N - 2\Delta_N^{(2)} + \frac{1}{4}(2m^2+M^2)(t-2M^2)J_N(M^2) - 4m^2M^2J_N^{(1)}(M^2) \right. \\
&\quad - M^2(t-2M^2)J_N^{(2)}(M^2) - \frac{1}{2}M^2(s-m^2+M^2)H(m^2) + \frac{1}{2}M^2(m^2+M^2-u)H^{(1)}(m^2) \\
&\quad + (4m^2+4M^2-t)H^{(2)}(m^2) - (2m^2+s-u)H^{(4)}(m^2) + \frac{(s-m^2-M^2)}{2} \left[ -H^{(2)}(s) \right. \\
&\quad - \frac{1}{2}(s-m^2+M^2)H^{(1)}(s) - (m^2-M^2)H^{(3)}(s) + \frac{1}{2}(s+3m^2+M^2-2t)J_N(M^2) \\
&\quad - M^2(s-m^2+M^2)H_B(s) - M^2(u-t)(H_B^{(1)}(s) + H_B^{(2)}(s)) - M^2(m^2-M^2)(3H_B^{(1)}(s) - H_B^{(2)}(s)) \\
&\quad + ((s-m^2)^2 - M^4)(H_B^{(1)}(s) - H_B^{(2)}(s)) + 2(9m^2-s+M^2-2t)H_B^{(3)}(s) \\
&\quad + (s-m^2-M^2)(5m^2-s-M^2-2t)(H_B^{(4)}(s) - H_B^{(6)}(s)) \\
&\quad \left. - (s-m^2-M^2)(m^2-s+3M^2-2t)(H_B^{(5)}(s) - H_B^{(6)}(s)) \right] \Big\} \\
&+ \frac{(c_3-c_4)mg^2}{F^4} \left\{ 2H^{(2)}(m^2) - \frac{1}{2}(s-m^2+M^2)H^{(3)}(s) + \frac{1}{2}(2M^2+s-u)J_N(M^2) \right. \\
&\quad - M^2 \left[ (2M^2+s-u)H_B^{(1)}(s) + (2m^2-s-u)H_B^{(2)}(s) \right] - 2(5m^2-s+M^2-t)H_B^{(3)}(s) \\
&\quad + (s-m^2-M^2)(2M^2+s-u)(H_B^{(4)}(s) - H_B^{(6)}(s)) - (s-m^2-M^2)(2m^2-s-u)(H_B^{(5)}(s) - H_B^{(6)}(s)) \Big\} \\
&+ \frac{c_4mg^2}{F^4} \left\{ -2\Delta_\pi + (s-m^2)(H^{(1)}(s) - 2H(s)) + 2(s+3m^2)(J_N(M^2) - M^2H_B(s)) \right. \\
&\quad \left. + 2(s-m^2)(s+3m^2-M^2)(H_B^{(1)}(s) - H_B^{(2)}(s)) \right\}, \\
B_{gh}^- &= -B_{gh}^+ \quad (c_4 = 0).
\end{aligned} \tag{C.11}$$

- Graph (k):

$$\begin{aligned}
A_k^+ &= -\frac{1}{6F^4} \left\{ 4c_1 M^2 \left[ 4\Delta_\pi + 3(-M^2 + 2t)J(t) \right] + 2c_3 \left[ -4M^2 \Delta_\pi + 3(2t - M^2) \left( \Delta_\pi + \left( \frac{t}{2} - M^2 \right) J(t) \right) \right] \right. \\
&\quad \left. + \frac{c_2}{m^2} \left[ -8m^2 \Delta_\pi^{(2)} + 3(2t - M^2) \left( \frac{1}{4} t^2 J(t) + 2 \left( m^2 - \frac{t}{4} \right) t J^{(1)}(t) - \frac{1}{2} t^2 J^{(2)}(t) \right) \right] \right\}, \\
A_k^- &= \frac{2c_4}{F^4} \left( m^2 + M^2 - s - \frac{t}{2} \right) t J^{(1)}(t), \\
B_k^+ &= 0 \\
B_k^- &= \frac{4c_4 m t J^{(1)}(t)}{F^4}
\end{aligned} \tag{C.12}$$

- Graph (m):

$$\begin{aligned}
A_m^+ &= \frac{3c_1 g^2 M^2}{F^4} \left\{ \Delta_\pi - 4m^2 H^{(1)}(m^2) - 4m^2 \left( J_N(t) - M^2 H_A(t) \right) \right\} \\
&\quad - \frac{3c_2 g^2}{4F^4} \left\{ \frac{2M^2 - t}{m^2} \Delta_\pi^{(2)} + (s - u)^2 H^{(3)}(m^2) - 4(2M^2 - t) H^{(4)}(m^2) - 2M^2 (s - u)^2 H_A^{(1)}(t) \right. \\
&\quad \left. + 2(s - m^2 - M^2)(m^2 + M^2 - u) \left[ \frac{1}{4m^2} \left( \Delta_\pi - 4m^2 H^{(1)}(m^2) \right) - H^{(5)}(m^2) + M^2 H_A(t) \right] \right. \\
&\quad \left. + 2t(4M^2 - t) J_N^{(1)}(t) + 2t^2 J_N^{(2)}(t) + M^2 \left[ 4(2M^2 - t) H_A^{(2)}(t) + 2(s - u)^2 H_A^{(3)}(t) - 2t^2 H_A^{(4)}(t) \right] \right\} \\
&\quad - \frac{3c_3 g^2}{4F^4} (2M^2 - t) \left\{ \Delta_\pi - 4m^2 H^{(1)}(m^2) - 4m^2 \left( J_N(t) - M^2 H_A(t) \right) \right\} \\
A_m^- &= -\frac{c_4 g^2 m^2 t (s - u) H_A^{(3)}(t)}{F^4} - \frac{s - u}{4m} B_m^-, \\
B_m^+ &= -\frac{6c_2 g^2}{F^4 m} \left\{ \frac{1}{2} (s - m^2 - M^2) + \frac{1}{2} (m^2 - u + M^2) \right\} \left( H^{(2)}(m^2) - H^{(4)}(m^2) \right) \\
B_m^- &= \frac{c_4 m g^2}{2F^4} \left\{ \Delta_\pi + 4m^2 \left[ -\frac{1}{2} J_N(t) - H^{(1)}(m^2) + M^2 H_A(t) - M^2 H_A^{(1)}(t) - 2H_A^{(2)}(t) \right. \right. \\
&\quad \left. \left. + (4m^2 - t) H_A^{(3)}(t) - t H_A^{(4)}(t) \right] \right\}
\end{aligned} \tag{C.13}$$

- Graphs (n)+(o)

$$\begin{aligned}
A_{no}^\pm &= \frac{2g^2}{F^4} \left\{ (c_1 M^2 + 2c_4 m^2) \left[ \Delta_N - M^2 H(m^2) \right] + (c_3 + c_4) m^2 \left[ 2H^{(2)}(m^2) - \frac{1}{2} (s - m^2 - M^2) H^{(3)}(m^2) \right] \right. \\
&\quad \left. + \frac{c_2}{16m^2} \left[ \left( s^2 - (m^2 - M^2)^2 \right) \left( \Delta_N - M^2 H^{(1)}(m^2) \right) - 8m^2 \Delta_N^{(2)} - M^2 (s - m^2 - M^2) \left( \Delta_\pi - M^2 \left( H(m^2) - H^{(1)}(m^2) \right) \right) \right. \right. \\
&\quad \left. \left. - 2(s + 3m^2 - M^2) \left( \Delta_\pi^{(2)} - (s - m^2 + 2M^2) H^{(2)}(m^2) \right) \right] \right\} \\
B_{no}^\pm &= -\frac{2mg^2}{(s - m^2)F^4} \left\{ (2c_1 M^2 + c_4 (s + 3m^2)) \left[ \Delta_N - M^2 H(m^2) \right] \right. \\
&\quad - \frac{c_2}{8m^2} \left[ 2(s + 3m^2) \Delta_N^{(2)} - \left( s^2 - (m^2 - M^2)^2 \right) \left( \Delta_N - M^2 H^{(1)}(m^2) \right) + M^2 (s - m^2 - M^2) \left( \Delta_\pi - M^2 \left( H(m^2) - H^{(1)}(m^2) \right) \right) \right. \\
&\quad \left. + 2(2s + 2m^2 - M^2) \left( \Delta_\pi^{(2)} - (s - m^2 + 2M^2) H^{(2)}(m^2) \right) \right] \\
&\quad \left. + (c_3 + c_4) \left[ (s + 3m^2) H^{(2)}(m^2) - m^2 (s - m^2 - M^2) H^{(3)}(m^2) \right] \right\}
\end{aligned} \tag{C.14}$$

- Graph (s):

$$\begin{aligned} A_s^\pm &= \frac{3g^2(s+3m^2)}{4F^4(s-m^2)} \left\{ 2c_1 M^2 \Delta_\pi - c_2 \frac{s}{m^2} \Delta_\pi^{(2)} - c_3 M^2 \Delta_\pi \right\}, \\ B_s^\pm &= -\frac{3g^2 m(s+m^2)}{F^4(s-m^2)^2} \left\{ 2c_1 M^2 \Delta_\pi - c_2 \frac{s}{m^2} \Delta_\pi^{(2)} - c_3 M^2 \Delta_\pi \right\}. \end{aligned} \quad (\text{C.15})$$

- Graph (v)

$$\begin{aligned} A_v^+ &= \frac{2}{3f^4} \left\{ 5c_1 M^2 \Delta_\pi - 2c_2 \left[ \frac{1}{4m^2} (s-m^2-M^2)(m^2-u+M^2) \Delta_\pi + \Delta_\pi^{(2)} \right] - c_3 (4M^2-t) \Delta_\pi \right\}, \\ A_v^- &= \frac{c_4(s-u) \Delta_\pi}{3F^4}, \\ B_v^+ &= 0, \quad B_v^- = -\frac{4c_4 m \Delta_\pi}{3F^4}. \end{aligned} \quad (\text{C.16})$$

#### Appendix D. Regular parts of scalar one-loop integrals

Following the method proposed by Refs. [6, 50], we have derived the regular parts of scalar integrals to the order needed by the  $O(p^4)$  calculation. All the results are listed except for the scalar integrals whose regular parts are equal to zero.

- 1 nucleon:

$$R_{01} = \frac{m^2}{16\pi^2} \left\{ R + \ln \frac{m^2}{\mu^2} \right\}. \quad (\text{D.1})$$

- 1 meson, 1 nucleon:

$$R_{11} = R_{11}^{(0)} + R_{11}^{(1)} + R_{11}^{(2)} + R_{11}^{(3)} + O(p^4) + \dots, \quad (\text{D.2})$$

where

$$\begin{aligned} R_{11}^{(0)} &= -\frac{1}{16\pi^2} \left\{ R - 1 + \ln \frac{m^2}{\mu^2} \right\}, \\ R_{11}^{(1)} &= \frac{s-m^2}{2m^2} \frac{1}{16\pi^2} \left\{ R - 1 + \ln \frac{m^2}{\mu^2} \right\}, \\ R_{11}^{(2)} &= \frac{1}{2} \left\{ \frac{M_\pi^2}{m^2} \frac{1}{16\pi^2} \left[ R + 3 + \ln \frac{m^2}{\mu^2} \right] - \left( \frac{s-m^2}{m^2} \right)^2 \frac{1}{16\pi^2} \left[ R + \ln \frac{m^2}{\mu^2} \right] \right\}, \\ R_{11}^{(3)} &= -\frac{1}{16\pi^2} \left\{ \frac{(s-m^2)M_\pi^2}{2m^4} \left[ R + 3 + \ln \frac{m^2}{\mu^2} \right] + \frac{(s-m^2)^3}{2m^6} \left[ R + \frac{1}{2} + \ln \frac{m^2}{\mu^2} \right] \right\}. \end{aligned}$$

- 2 nucleons:

$$R_{02} = R_{02}^{(0)} + R_{02}^{(2)} + O(p^4) + \dots, \quad (\text{D.3})$$

where

$$\begin{aligned} R_{02}^{(0)} &= -\frac{1}{16\pi^2} \left\{ R + 1 + \ln \frac{m^2}{\mu^2} \right\}, \\ R_{02}^{(2)} &= \frac{t}{96\pi^2 m^2}. \end{aligned}$$

- 2 mesons, 1 nucleon:

$$R_{21} = R_{21}^{(0)} + R_{21}^{(2)} + O(p^4) + \dots, \quad (\text{D.4})$$

where

$$\begin{aligned} R_{21}^{(0)} &= -\frac{1}{32\pi^2 m^2} \left\{ R + 3 + \ln \frac{m^2}{\mu^2} \right\}, \\ R_{21}^{(2)} &= \frac{1}{32\pi^2 m^2} \left\{ \frac{2M_\pi^2}{3m^2} - \frac{t}{6m^2} \left[ R + \frac{11}{3} + \ln \frac{m^2}{\mu^2} \right] \right\}. \end{aligned}$$

- 1 meson, 2 nucleons (Case A):

$$R_A = R_A^{(0)} + R_A^{(2)} + O(p^4) + \dots, \quad (\text{D.5})$$

where

$$\begin{aligned} R_A^{(0)} &= \frac{1}{32\pi^2 m^2} \left\{ R + 1 + \ln \frac{m^2}{\mu^2} \right\}, \\ R_A^{(2)} &= \frac{1}{32\pi^2 m^2} \left\{ \frac{t}{6m^2} \left[ R + \ln \frac{m^2}{\mu^2} \right] - \frac{M_\pi^2}{m^2} \right\}. \end{aligned}$$

- 1 meson, 2 nucleons (Case B):

$$R_B = R_B^{(0)} + R_B^{(1)} + R_B^{(2)} + O(p^3) + \dots, \quad (\text{D.6})$$

where

$$\begin{aligned} R_B^{(0)} &= \frac{1}{32\pi^2 m^2} \left\{ R + 1 + \ln \frac{m^2}{\mu^2} \right\}, \\ R_B^{(1)} &= -\frac{s-m^2}{2m^2} \frac{1}{32\pi^2 m^2} \left\{ R + 2 + \ln \frac{m^2}{\mu^2} \right\}, \\ R_B^{(2)} &= \frac{1}{32\pi^2 m^2} \left\{ \frac{M_\pi^2}{m^2} \left[ \frac{1}{6} \left( R + \ln \frac{m^2}{\mu^2} \right) - 1 \right] - \frac{1}{6} \left( \frac{s-m^2}{m^2} \right)^2 \left[ R + \frac{3}{2} + \ln \frac{m^2}{\mu^2} \right] \right\}. \end{aligned}$$

- 3 nucleons:

$$R_{03} = R_{03}^{(0)} + R_{03}^{(2)} + O(p^4) + \dots, \quad (\text{D.7})$$

where

$$\begin{aligned} R_{03}^{(0)} &= \frac{1}{32\pi^2 m^2}, \\ R_{03}^{(2)} &= \frac{1}{6} \frac{1}{32\pi^2 m^2} \left\{ \frac{t}{2m^2} + \frac{M_\pi^2}{m^2} \right\}. \end{aligned}$$

- 1 meson, 3 nucleons:

$$R_{13} = R_{13}^{(0)} + R_{13}^{(1)} + O(p^2) + \dots, \quad (\text{D.8})$$

where

$$\begin{aligned} R_{13}^{(1)} &= -\frac{1}{32\pi^2 m^4}, \\ R_{13}^{(2)} &= \frac{s-m^2}{m^2} \frac{1}{32\pi^2 m^4}. \end{aligned}$$

## Appendix E. Renormalization of the effective couplings

- $\overline{\text{MS}} - 1$  renormalized LECs:

$$c_i = c_i^r(\mu) + \frac{\gamma_i^c m R}{16\pi^2 F^2}, \quad d_j = d_j^r(\mu) + \frac{\gamma_j^d R}{16\pi^2 F^2}, \quad e_k = e_k^r(\mu) + \frac{\gamma_k^e R}{16\pi^2 F^2 m},$$

$$\begin{aligned} \gamma_1^c &= -\frac{3}{8}g^2 + \frac{9}{2}c_1 g^2 m, \\ \gamma_2^c &= \frac{1}{2} - g^2 + \frac{g^4}{2} + \left[ -\frac{2c_4}{3} + \frac{1}{6}(3c_2 + 8c_3 + 4c_4)g^2 \right] m, \\ \gamma_3^c &= \frac{1}{4} - \frac{3g^2}{2} + \frac{g^4}{4} + \left[ \frac{5c_4}{3} + \frac{1}{12}(-3c_2 + 54c_3 - 52c_4)g^2 \right] m, \\ \gamma_4^c &= \frac{1}{4} - \frac{g^2}{2} + \frac{g^4}{4} + \left[ c_4 + \frac{1}{12}(-13c_2 + 8c_3 - 12c_4)g^2 \right] m, \end{aligned}$$

$$\begin{aligned} \gamma_1^d + \gamma_2^d &= \frac{1}{48} - \frac{g^2}{12} + \frac{g^4}{16} + \left[ \frac{1}{24}(7c_2 + 16c_3 - 10c_4) + \frac{1}{48}(34c_2 - 32c_3 + 4c_4)g^2 \right] m, \\ \gamma_3^d &= \frac{5}{6}c_2(1 - g^2)m, \\ \gamma_5^d &= \frac{1}{48} - \frac{g^2}{48} + \left[ \frac{1}{48}(-72c_1 - 3c_2 + 8c_3 + 4c_4) + \frac{1}{48}(48c_1 - 4c_3 + 2c_4)g^2 \right] m, \\ \gamma_{14}^d - \gamma_{15}^d &= \frac{1}{4} - \frac{g^2}{2} + \frac{g^4}{4} + \left[ c_4 + \frac{1}{12}(-13c_2 + 8c_3 - 12c_4)g^2 \right] m, \\ \gamma_{18}^d &= \frac{1}{12}(24c_1 + c_2 - 4c_3 - 4c_4)gm. \end{aligned}$$

$$\begin{aligned} \gamma_{14}^e &= \frac{1}{64} - \frac{g^2}{32} + \frac{g^4}{64} + \left[ \frac{1}{48}(-2c_2 - 12c_3 - 5c_4) + \frac{1}{192}(-13c_2 + 8c_3 + 20c_4)g^2 \right] m, \\ \gamma_{15}^e &= \frac{1}{12}c_2 g^2 m, \\ \gamma_{16}^e &= 0, \\ \gamma_{17}^e &= \frac{1}{192} - \frac{g^2}{48} + \frac{g^4}{64} + \left[ \frac{1}{96}(-c_2 + 2c_4) + \frac{7}{96}(3c_2 - 2c_4)g^2 \right] m, \\ \gamma_{18}^e &= \frac{1}{8}c_2(1 - g^2)m, \\ 2\gamma_{19}^e - \gamma_{22}^e - \gamma_{36}^e &= \frac{1}{16} - \frac{g^2}{8} + \frac{g^4}{16} + \left[ c_1 - \frac{5c_2}{48} + \frac{3c_3}{8} + \frac{c_4}{3} + \frac{1}{48}(21c_2 + 26c_3 - 16c_4)g^2 \right] m, \\ \gamma_{20}^e + \gamma_{35}^e &= \frac{1}{24}c_2(6 - g^2)m, \\ 2\gamma_{21}^e - \gamma_{37}^e &= \frac{1}{48} - \frac{g^2}{48} + \left[ \frac{1}{48}(-24c_1 + c_2 + 16c_3) + \frac{1}{24}(-3c_2 - 6c_3 + 14c_4)g^2 \right] m, \\ \gamma_{22}^e - 4\gamma_{38}^e &= -\frac{1}{32} + \frac{g^2}{16} - \frac{g^4}{32} + \left[ \frac{1}{24}(-36c_1 + 3c_2 + 9c_3 + c_4) + \frac{1}{96}(-72c_1 - 21c_2 - 4(2c_3 + c_4))g^2 \right] m. \end{aligned}$$

- EOMS renormalized LECs:

$$c_i^r = \widetilde{c}_i + \frac{\delta_i^c m}{16\pi^2 F^2}, \quad d_j^r = \widetilde{d}_j + \frac{\delta_j^d}{16\pi^2 F^2},$$

$$\begin{aligned}
\delta_1^c &= \frac{3g^2}{8} + 3c_1 g^2 m, \\
\delta_2^c &= -1 - \frac{g^4}{2} + \left[ -\frac{2c_4}{9} + \frac{1}{9}(9c_2 + 16c_3 + 14c_4)g^2 \right] m, \\
\delta_3^c &= \frac{9g^4}{4} + \left[ \frac{2c_4}{9} + \frac{1}{72}(-9c_2 + 216c_3 - 272c_4)g^2 \right] m, \\
\delta_4^c &= -\frac{5g^2}{4} - \frac{g^4}{4} + \left[ -\frac{1}{72}(9c_2 + 32c_3 + 16c_4) + \frac{1}{72}(9c_2 - 88c_4)g^2 \right] m, \\
\delta_1^d + \delta_2^d &= -\frac{1}{36} \left[ (4c_2 + 10c_3 + 5c_4) + (8c_2 - 22c_3 + 38c_4)g^2 \right] m, \\
\delta_3^d &= \frac{1}{18} \left[ (-34c_2 - 30c_3 + 3c_4) + (4c_2 + 15c_4)g^2 \right] m, \\
\delta_5^d &= \frac{1}{72} \left[ (144c_1 - 2c_3 - c_4) + (72c_1 - 38c_3 + 10c_4)g^2 \right] m, \\
\delta_{14}^d - \delta_{15}^d &= \left[ \frac{c_4}{3} + \frac{1}{72}(67c_2 - 56c_3 + 96c_4)g^2 \right] m, \\
\delta_{18}^d &= \frac{1}{9}(c_2 - c_3 - c_4)gm.
\end{aligned}$$

## Appendix F. The effect of unitarity

The phase shift formula Eq. 33 for a perturbative amplitude automatically includes the effect of unitarity in an obscure way. This is illustrated in this section.

The partial wave phase shift for an amplitude, satisfying the elastic unitarity relation exactly, can be obtained via Eq. 32, which reads

$$\delta_{\ell\pm}^I = \arctan \left\{ \frac{\text{Im} f_{\ell\pm}^I}{\text{Re} f_{\ell\pm}^I} \right\}. \quad (\text{F.1})$$

Nevertheless, for a perturbative amplitude the unitarity relation may be violated. In section 2.6, we follow Ref. [10] to define the phase shift presented by Eq. 33. Hence, starting from a perturbative amplitude, one may have several methods to calculate the phase shift. For instance:

- Method 1: perturbative ampl.  $f^P \xrightarrow{\text{Eq. 33}} \delta^P = \arctan \{ |\vec{p}| \text{Re} f^P \}$ .
- Method 2: perturbative ampl.  $f^P \xrightarrow{\text{unitarization using K-Matrix method}} \text{unitarized ampl. } f^K \rightarrow \delta^K = \arctan \left\{ \frac{\text{Im} f^K}{\text{Re} f^K} \right\}$ .

Here the K-Matrix approach is employed to unitarize the perturbative amplitude, one can also adopt other approaches of unitarization.  $f^P$  and  $f^K$  denote the perturbative amplitude and the K-Matrix unitarized amplitude, respectively.  $\delta^P$  stands for the phase shift calculated via Eq. 33 with  $f^P$ , while  $\delta^K$  presents the one calculated via Eq.32 with  $f^K$ . Note that the indices for isospin and angular momentum are suppressed hereafter. In our paper, Method 1 has been adopted to calculate the phase shift. Below we take the perturbative  $\pi$ -N scattering amplitude up to  $O(p^4)$  without the  $\Delta(1232)$  contribution for example to demonstrate that  $\delta^P = \delta^K$ .

The chiral perturbative  $\pi$ -N scattering partial wave amplitude at  $O(p^4)$  is expressed by

$$f^P(s) = f^{(1)}(s) + f^{(2)}(s) + f^{(3)}(s) + f^{(4)}(s). \quad (\text{F.2})$$

Using the K-Matrix approach, the unitarized amplitude that obeys the unitarity relation takes the following form,

$$f^K(s) = \frac{f^{(1)}(s) + f^{(2)}(s) + \text{Re}f^{(3)}(s) + \text{Re}f^{(4)}(s)}{1 - i|\vec{p}|(f^{(1)}(s) + f^{(2)}(s) + \text{Re}f^{(3)}(s) + \text{Re}f^{(4)}(s))} , \quad (\text{F.3})$$

where  $f^{(1)}(s)$  and  $f^{(2)}(s)$  stand for the contributions from the  $O(p)$  and  $O(p^2)$  tree amplitudes, respectively. The fact that  $\text{Re}f^{(1)}(s) = f^{(1)}(s)$  and  $\text{Re}f^{(2)}(s) = f^{(2)}(s)$  has been used to get Eq. F.3. The phase shift obtained through Method 1 reads

$$\delta^P = \arctan \left\{ |\vec{p}| \text{Re}f^P(s) \right\} = \arctan \left\{ |\vec{p}| \left[ f^{(1)}(s) + f^{(2)}(s) + \text{Re}f^{(3)}(s) + \text{Re}f^{(4)}(s) \right] \right\} , \quad (\text{F.4})$$

while the one obtained through Method 2 reads

$$\delta^K = \arctan \left\{ \frac{\text{Im}f^K(s)}{\text{Re}f^K(s)} \right\} = \arctan \left\{ |\vec{p}| \left[ f^{(1)}(s) + f^{(2)}(s) + \text{Re}f^{(3)}(s) + \text{Re}f^{(4)}(s) \right] \right\} . \quad (\text{F.5})$$

Thus,  $\delta^P = \delta^K$ . A numerical calculation we performed also supports this observation. Hence in our work the effect of unitarity has already been included when performing fits to the partial wave shift data in Section 3.1. The phase shift formula Eq. 33 for the perturbative amplitude is reasonable in the sense that it takes the effect of unitarity into consideration automatically. The phase shift calculated via Eq. 33 using the perturbative amplitude and the one via Eq. 32 using the K-Matrix unitarized amplitude are the same, which is true at least for the calculation up to  $O(p^4)$  in this paper.

Nevertheless, the advantage of the unitarized amplitude can be shown by plotting the real part of the unitarized amplitude, the one of the perturbative amplitude and the unitary bound together, e.g. see Fig. F.14 for the  $P_{33}$  partial wave.

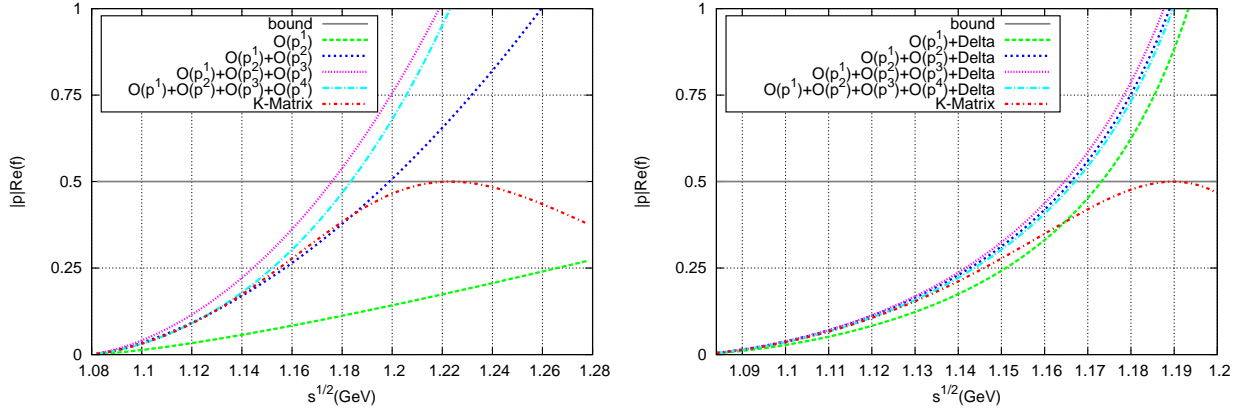


Figure F.14: Unitarity bound for the real part of the  $P_{33}$  partial wave amplitude. Left: without the  $\Delta(1232)$  contribution; Right: with the  $\Delta(1232)$  contribution. The results from Table 3 are adopted for plotting.

## Appendix G. The effect of the $\Delta(1232)$ width

In section 3.2, when the  $\Delta(1232)$  is included explicitly, the phase shift is obtained through Method 1 discussed in Appendix F,

$$\delta^P = \arctan \left\{ |\vec{p}| \text{Re}f^P(s) \right\} = \arctan \left\{ |\vec{p}| \left[ f^{\Delta, \text{Born}}(s) + f^{(1)}(s) + f^{(2)}(s) + \text{Re}f^{(3)}(s) + \text{Re}f^{(4)}(s) \right] \right\} , \quad (\text{G.1})$$

where  $f^{\Delta, \text{Born}}(s)$  represents the LO Born term contribution (see Eq. A.3) without an explicit  $\Delta$  width in the propagator. According to the discussion shown in Appendix F, it is equivalent to calculate the phase shift via a K-Matrix

unitarized amplitude

$$f^K(s) = \frac{f^{\Delta, \text{Born}}(s) + f^{(1)}(s) + f^{(2)}(s) + \text{Re}f^{(3)}(s) + \text{Re}f^{(4)}(s)}{1 - i|\vec{p}|(f^{\Delta, \text{Born}}(s) + f^{(1)}(s) + f^{(2)}(s) + \text{Re}f^{(3)}(s) + \text{Re}f^{(4)}(s))} . \quad (\text{G.2})$$

If one forgets  $f^{(1)}(s) + f^{(2)}(s) + \text{Re}f^{(3)}(s) + \text{Re}f^{(4)}(s)$  for a while , then

$$f^K(s) = \frac{f^{\Delta, \text{Born}}(s)}{1 - i|\vec{p}|(f^{\Delta, \text{Born}}(s))} . \quad (\text{G.3})$$

The above equation contains an infinite resummation of Feynman diagrams shown in Fig. G.15. This resummation will generate the  $\Delta(1232)$  width properly.

On the other hand, one can add to the  $\Delta$  propagator in the  $f^{\Delta, \text{Born}}(s)$  an explicit width given by Ref.[41],

$$\Gamma(s) = 2 \left( \frac{h_A}{2F_\pi} \right)^2 \frac{s + m_N^2 - M_\pi^2}{24\pi m_\Delta^2} |\vec{p}|^3 . \quad (\text{G.4})$$

This provides us a LO Born term  $\Delta$ -exchange contribution with the explicit  $\Delta$  width, which we denote it by  $f^{\Delta\Gamma, \text{Born}}(s)$ . Using Eq. 32, we have checked that the effect of  $f^K(s)$  is almost the same as that of  $f^{\Delta\Gamma, \text{Born}}(s)$ .

Now taking  $f^{(1)}(s) + f^{(2)}(s) + \text{Re}f^{(3)}(s) + \text{Re}f^{(4)}(s)$  into consideration, one can observe that the resummation shown in Fig. G.15 still exists though many new terms of different types appear. To conclude, in our work, the dominant effect of the  $\Delta$  width is included through Method 1, namely through the phase shift formula Eq. 33 for the  $\pi$ -N perturbative amplitude, when performing fits to phase shift up to 1.2 GeV.

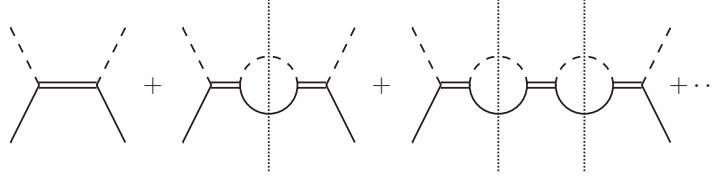


Figure G.15: Resummation to generate the  $\Delta(1232)$  width. The solid, dashed and double solid lines represent the nucleon, pion and  $\Delta(1232)$ , respectively. The vertical dotted lines show that the nucleon and pion in the loops are on mass shell.

## References

- [1] G. Hohler, in Landolt-Börnstein, **9b2**, ed. H. Schopper, Springer, Berlin, (1983).
- [2] S. Weinberg, Physica A **96**, 327 (1979).
- [3] J. Gasser and H. Leutwyler, Annals Phys. **158** 142 (1984).
- [4] J. Gasser, M. E. Sainio and A. Svarc, Nucl. Phys. **B307**, 779 (1988).
- [5] E. E. Jenkins and A. V. Manohar, Phys. Lett. B **255**, 558 (1991).
- [6] T. Becher and H. Leutwyler, Eur. Phys. J. C **9**, 643 (1999).
- [7] J. Gegelia and G. Japaridze, Phys. Rev. D **60**, 114038 (1999).
- [8] T. Fuchs, J. Gegelia, G. Japaridze and S. Scherer, Phys. Rev. D **68**, 056005 (2003).
- [9] M. Mojziz, Eur. Phys. J. C **2**, 181 (1998).
- [10] N. Fettes, U. -G. Meissner and S. Steininger, Nucl. Phys. A **640**, 199 (1998).
- [11] N. Fettes and U. -G. Meissner, Nucl. Phys. A **676**, 311 (2000).
- [12] T. Fuchs, J. Gegelia and S. Scherer, Eur. Phys. J. A **19**, 35 (2004).
- [13] V. Bernard, N. Kaiser and U. -G. Meissner, Int. J. Mod. Phys. E **4**, 193 (1995).
- [14] P. J. Ellis and H. B. Tang, Phys. Rev. C **57**, 3356 (1998).
- [15] J. Gegelia, G. S. Japaridze, and K. S. Turashvili, Theor. Math. Phys. **101**, 1313 (1994).
- [16] T. Becher and H. Leutwyler, JHEP **0106**, 017 (2001).
- [17] K. Torikoshi and P. J. Ellis, Phys. Rev. C **67**, 015208 (2003).
- [18] J. M. Alarcon, J. Martin Camalich, J. A. Oller and L. Alvarez-Ruso, Phys. Rev. C **83**, 055205 (2011).
- [19] L. S. Geng, J. Martin Camalich, L. Alvarez-Ruso and M. J. Vicente Vacas, Phys. Rev. Lett. **101**, 222002 (2008).
- [20] J. M. Alarcon, J. Martin Camalich and J. A. Oller, Phys. Rev. D **85**, 051503 (2012).
- [21] J. M. Alarcon, J. Martin Camalich and J. A. Oller, Prog. Part. Nucl. Phys. **67**, 375 (2012) .



- [22] J. Martin Camalich, J. M. Alarcon and J. A. Oller, Prog. Part. Nucl. Phys. **67**, 327 (2012) .
- [23] J. M. Alarcon, J. M. Camalich and J. A. Oller, arXiv:1210.4450 [hep-ph].
- [24] M. Hoferichter, B. Kubis and U. G. Meiner, Nucl. Phys. A **833**, 18 (2010).
- [25] V. Baru, C. Hanhart, M. Hoferichter, B. Kubis, A. Nogga and D. R. Phillips, Phys. Lett. B **694**, 473 (2011).
- [26] J. J. de Swart, M. C. M. Rentmeester and R. G. E. Timmermans, PiN Newslett. **13**, 96 (1997).
- [27] A. Bottino, F. Donato, N. Fornengo, S. Scopel, Phys. Rev. D **78**, 083520 (2008).
- [28] J. R. Ellis, K. A. Olive, C. Savage, Phys. Rev. D **77**, 065026 (2008).
- [29] X. L. Ren, L. S. Geng, J. Martin Camalich, J. Meng and H. Toki, nucl-th/1209.3641.
- [30] J. Gasser, H. Leutwyler and M. E. Sainio, Phys. Lett. B **253**, 252 (1991).
- [31] M. Procura, T. R. Hemmert and W. Weise, Phys. Rev. D **69**, 034505 (2004).
- [32] N. Fettes, U. -G. Meissner, M. Mojzis and S. Steininger, Annals Phys. **283**, 273 (2000) .
- [33] M. R. Schindler, CITATION = INSPIRE-745798;
- [34] G. Passarino and M. J. G. Veltman, Nucl. Phys. B **160**, 151 (1979).
- [35] A. I. Davydychev, Phys. Lett. B **263**, 107 (1991).
- [36] Y. H. Chen, D. L. Yao and H. Q. Zheng, arXiv:1207.7212 [hep-ph]; Talk given by D. L. Yao at *QCD2012*, July 2- 7, Montpellier, France.
- [37] V. Pascalutsa and M. Vanderhaeghen, Phys. Lett. B **636**, 31 (2006).
- [38] M. R. Schindler, T. Fuchs, J. Gegelia and S. Scherer, Phys. Rev. C **75**, 025202 (2007).
- [39] S. -i. Ando and H. W. Fearing, Phys. Rev. D **75**, 014025 (2007).
- [40] R. A. Arndt, W. J. Briscoe, I. I. Strakovsky, R. L. Workman, Phys. Rev. C **74**, 045205 (2006) .  
R. A. Arndt, et al. The SAID program, <http://gwdac.phys.gwu.edu>.
- [41] V. Pascalutsa and D. R. Phillips, Phys. Rev. C **67**, 055202 (2003) .
- [42] V. Pascalutsa, Phys. Lett. B **503**, 85 (2001).
- [43] V. Pascalutsa, M. Vanderhaeghen and S. N. Yang, Phys. Rept. **437**, 125 (2007).
- [44] M. L. Goldberger and S. B. Treiman, Phys. Rev. **110**, 1178 (1958).  
M. L. Goldberger and S. B. Treiman, Phys. Rev. **111**, 354 (1958).
- [45] S. Aoki *et al.* (PACS-CS Collaboration), Phys. Rev. D **79**, 034503 (2009).
- [46] A. Walker-Loud *et al.*, Phys. Rev. D **79**, 054502 (2009).
- [47] H.-W. Lin *et al.* (HSC Collaboration), Phys. Rev. D **79**, 034502 (2009).
- [48] W. Bietenholz *et al.* (QCDSF-UKQCD Collaboration), Phys. Rev. D **84**, 054509 (2011).
- [49] S. R. Beane *et al.* (NPLQCD Collaboration), Phys. Rev. D **84**, 014507 (2011).
- [50] M. R. Schindler, J. Gegelia and S. Scherer, Phys. Lett. B **586**, 258 (2004).